#51

Please return to
Marc Meyers
Met. Dept.

51

To be published in "Explosive Welding, Forming, and Compaction"
Applied Science Publishers
Ed. T.Z. Blazynski

CHAPTER 3

METALLURGICAL EFFECTS OF SHOCK AND PRESSURE WAVES IN METALS

L.E. Murr

Oregon Graduate Center
19600 N.W. Walker Road
Beaverton, Oregon 97006

and

M.A. Meyers

Department of Metallurgical and Materials Engineering
New Mexico Institute of Mining and Technology
Socorro, New Mexico 87801

I. PRINCIPAL FEATURES OF HIGH-STRAIN-RATE AND SHOCK DEFORMATION IN METALS

It is a well-known fact that the mechanical response of metals depends upon the temperature, the velocity of deformation, the previous deformation undergone, and the stress state, among other parameters. As a result, various attempts have been made to incorporate these parameters into a single equation that would have the capability of predicting the response of a specific metal under a wide range of circumstances. By analogy with thermodynamics, this equation is referred to as the "mechanical equation of state"

$$f(\sigma, \varepsilon, \dot{\varepsilon}, T) = 0 \tag{1}$$

Changes in stress can be expressed as:

$$d\sigma = \left(\frac{\partial \sigma}{\partial \varepsilon}\right)_{\dot{\varepsilon},T} d\varepsilon + \left(\frac{\partial \sigma}{\partial \dot{\varepsilon}}\right)_{\varepsilon,T} d\dot{\varepsilon} + \left(\frac{\partial \sigma}{\partial T}\right)_{\varepsilon,\dot{\varepsilon}} dT, \tag{2}$$

However, plastic deformation is, by definition, an irreversible process, and the thermodynamic equation of state, from which Eq. 2 was obtained, only strictly applies to reversible processes. Hence, Eq. 2 can only be accepted as an approximate formulation, and the term "mechanical modelling" is perhaps more appropriate than mechanical equation of state. Both Hart[2] and Rohde[3] have proposed models.

The general trend observed is that the flow stress increases with strain rate increase and temperature decrease. The reason for this flow stress increase seems to be connected to a decreasing ability of thermal energy to aid dislocation movement at higher strain rates and lower temperatures. Figure 1 shows a

stress-strain-strain rate plot for mild steel[4]. The yield stress increases from 33 to 60 ksi, as the strain rate is varied from 10^{-4} to 10^{2}. However, the strain-rate sensitivity of different materials is different, and the exponent in the equation below has been found to vary significantly

$$\sigma = k\,(\dot{\varepsilon})^{m} \qquad (3)$$

where m is called the strain-rate sensitivity. This dependence of mechanical properties upon strain rate is described in detail by Campbell[4]. An example of a material that does not virtually exhibit any strain-rate sensitivity is given in Fig. 2. A 6061-T6 aluminum was tested at strain rates of 9×10^{-3}, 15×10^{-2}, 2, 40, and 210 s^{-1} and the stress-strain curves are identical[5]. A number of experimental techniques have been designed to determine the mechanical response of metals over this wide strain-rate range. For rates of 1 s^{-1} or lower, the quasi-static universal testing machines are appropriate. In the $1 - 10^{4}$ s^{-1} range, special testing machines have been developed. They are briefly described below[5]:

a) Pneumatic machine. This consists of a gas-driven piston; this piston has a low mass so that it can be rapidly accelerated to its steady state velocity. The machine built by Maiden and Green[5] has a response time of 100 - 200 μs and allows a maximum strain rate of $20s^{-1}$. A variation of this machine is the biaxial preumatic machine described by Lindholm[6], Lindholm and Yearley[7].

b) Rotating flywheel machine. A flywheel rotating at a constant velocity transmits the energy to the specimen by a

hammer that is spring loaded. A more modern version of this instrument, in which the flywheel is shaped like a cam, has the advantage of avoiding the impact; the cam is continuously in contact with the specimen. It is called a cam plastimeter. Another similar instrument was built by Culver[8,9]; he called it a "torsional impact apparatus".

c) Expanding ring test[10]. A metallic ring is expanded by means of an explosive charge. The stress, strain, and strain rate are recorded and/or calculated as the ring expands.

d) Hopkinson bar[11,12]. In this technique, a cylindrical specimen is placed between two long cylindrical bars. An elastic wave, upon traversing the bar, enters the specimen. The amplitude of the wave is such as to plastically deform the specimen.

The above testing techniques, which cover the $1\text{-}10^4 s^{-1}$ range of strain rates, assume that the stress is uniformly distributed in the specimen. Higher strain rates ($10^6 s^{-1}$) are present in shock waves; in this case, however, the stress propagates as a discontinuity in the specimen (shock front) and the situation is fundamentally different. Several techniques have been developed for shock-loading experiments: two-stage gas guns, explosively-driven impact of flyer plates, detonation of explosive in contact with metal, among others.

It is important to know the strain-rate dependence of the mechanical response of metals because a large number of mechanical fabrication techniques use strain rates much above those usually employed in conventional tensile testing. Campbell[4] cites some typical strain rates; in machining it is about $10^5 s^{-1}$;

in sheet, rod or wire drawing, it varies between 1 and $10^3 s^{-1}$ in deep drawing, it may be as high as $10^2 s^{-1}$. However, it is in high-energy rate processes that the strain-rates are typically and systematically high (10^2 to $10^4 s^{-1}$). Figure 3 shows the various explosive metal-working processes, which comprise an important part of the high energy rate fabrication processes. One has, in essence, three types of operations: standoff, contact, and impact. In the standoff operations, there is a medium that transfers the energy from the explosive to the workpiece (usually water). The magnitude of the pressure generated in the workpiece is not high enough to generate shock waves (in general). Contact and impact operations, on the other hand, generate high pressures and shock waves in the workpiece. One can see that one can have a whole range of strain rates and deformation regimes in explosive metal working.

A phenomenon of considerable practical importance in explosive forming is the increased ductility exhibited by a number of alloys at high strain rates. This results in an improved formability; the retardation of necking occurs at a certain deformation velocity, as shown in Fig. 4. Especially noteworthy is the increased ductility of 17-7 pH stainless steel. Orava[14] interpreted this increased ductility as related to the onset of plastic stress wave propagation. He suggested that, when the impact velocity is such that a stress-wave travels through the system has an amplitude equal to the dynamic yield stress of the material, ductility increases. At this stress level the plastic deformation takes place at the wave front and the effective

strain rate undergoes a significant increase over the one that one would expect if deformation were uniformly distributed over the specimen.

As one can see from the above, it is very difficult to predict a priori the medium of deformation under the imposed conditions. Additional complicating factors are introduced by the strain-rate dependence of the substructure morphology. Dislocations, deformation twins, phase transformations are all affected by the strain rate and strain state. They are discussed in the previous chapter. An effect that is being increasingly recognized as important is adiabatic shearing. This effect is simple to explain in general terms; however, the specific mechanisms are only partially understood. Zener and Hollomon[15] were the first to describe it. Recently it has received a great deal of attention[16-21]. Olson et al[16] defined an adiabatic shear band as a strain-localization phenomenon that is generally attributed to a plastic instability arising from a thermal softening effect during adiabatic or near-adiabatic plastic deformation. In other words, as the strain rate is increased the deformation tends more and more towards an adiabatic state. Hence, if for a certain reason one has localized deformation, the temperature will increase at that region, above the average temperature. Since the flow stress decreases with temperature, the hotter region will undergo more and more deformation. This localization of deformation produces bands. One example of shear band formation is shown in Fig. 5. Depending on the temperature achieved, the rate of cooling (after

deformation), and the composition of the alloy, the adiabatic shear band can present different characteristics. Moss[20] found that the shear strain across a band could be as high as 572. The shear strain rate inside a band was found to go up to 9.4×10^7 s^{-1}. Rogers and Shastry[19] discussed the phase transformation occurring within the shear bands when either the strain concentration or strain rate are sufficiently large. The deformation mechanism responsible for adiabatic shear bands is still not very well understood, but it is doubtful that dislocations play a preponderant role. Indeed, Olson et al[16] have discussed an alternative mechanism, involving the formation and reclosure of shear cracks in the material. This mechanism seems to have a great potential, since nothing would impede crack reclosure, under the high stresses, and temperatures; and since no oxidation of the fracture surfaces would be allowed.

At strain rates up to 10^4, one considers the stress as uniformly distributed over the length of the specimen (workpiece). At these velocities of deformation the inertia of the system becomes more and more important, and elastic and plastic waves propagating through the specimen might obscure the results. The upper limit for the strain rate is given by shock loading. In this situation, the strain is imparted by the passage of a shock wave throughout the specimen. Hence, one has a non-uniform distribution of stresses and strains during the deformation process.

As demonstrated in the previous chapter, the passage of a shock wave in a solid crystalline material can be fairly

rigorously described in a phenomenological and mechanical way. However its interaction with any specific structure is sometimes complicated by very subtle features which promote specific residual microstructures.

The propagation of a shock wave in a metal or alloy is shown schematically in Fig. 6(a). The deformation induced in a solid metal or alloy by a shock wave having a shape as shown in Fig. 6(a) can be separated into three prominent parts or regions: compression of the solid by the shock front (I), a region of constant peak pressue where no overall volume work is done, and which defines the shock pulse (II), and a rarefaction (relief) portion (III). Since $dV = 0$ in region II, the major contributions to shock deformation producing permanent, residual microstructural phenomena must come from the compression (I) and relief portions (III) of the shock wave. One can estimate the strain rate at the shock front in an approximate way. A pressure of 20 GPa generates a shear strain of 0.10 for a metal such as copper. The rise-time of the shock front has not been accurately determined as yet, but can be estimated to be equal to 0.1 s (or less). The strain rate obtained by dividing these two values is $10^6 s^{-1}$, At the rarefaction part of the wave, the strain rate is lower by about an order of magnitude. While the internal energy change across the shock front is calculated assuming an adiabatic process, the work done on the solid during rarefaction is calculated assuming an isentropic relief process[2], according to the hydrodynamic theory, that assumes that the solid acts like a fluid. Consequently, the total change in internal energy after

shock compression is expressed as[22]:

$$(E_f - E_0) = [(P_i + P_0)(V_0 - V_i)]/2 - \int_{V_i}^{V_f} P_s(V)\, dV \qquad (4)$$

where E_f and V_f are the final values and P_i and V_i are intermediate values associated with the peak pressure, and $P_s(V)$ is the isentropic relief path.

Grace [23] has expressed the elastic energy stored by means of defects as a function of the pressure, but Eq. 4 cannot be applied because it does not take into account the additional processes taking place in crystalline solids. Indeed, Hsu et al[24] have shown that the hydrodynamic model does not apply to nickel and that one has additional heating (above that predicted by the hydrodynamic model), dislocations and point defects; consequently, one has to add a term taking into account these additional processes

$$(E_f - E_0) = [(P_i + P_0)(V_0 - V_i)]/2 - \int_{V_i}^{V_f} P_s(V)\, dV + E_s \qquad (5)$$

where E_s is the energy stored as defects or additional heating.

Nevertheless, one can illustrate how shock waves having specific peak pressures can alter the metallurgical (microstructural, physical, and mechanical) properties of metals by correlating the energy stored in the material with the elastic strain energy due to defects. Grace used the following equation:

$$\sigma = \sigma_0 + 2\,\alpha\, G|\underset{\sim}{b}|(W^E)^{1/2} \qquad (6)$$

where α is a constant, G is the shear modulus, $\underset{\sim}{b}$ is the lattice

dislocation Burgers vector, σ_o is the initial yield stress (prior to shock-wave propagation). This expression is intended as an illustration of the overall response of a metal or alloy to the stored energy induced by shock-wave passage. The specific form will change depending upon the particular types of defects contributing to the stored energy.

In Eq. 5, one can decompose E_s into E_{s1}, the energy due to defects, and E_{s2}, the heating over and above that predicted by the hydrodynamic theory. Hence:

$$E_{s1} = (E_f - E_o - E_{s2}) - [(P_i + P_o)(V_o - V_i)]/2 + \int_{V_i}^{V_f} P_s(V)dV \quad (7)$$

$$;(E_f - E_o - E_{s2}) = C_R\Delta T$$

But E_{s1} is equal to W^E, and one has on substituting Eq. 7 into Eq. 6:

$$\sigma = \sigma_o + 2\alpha G|\underset{\sim}{b}|\left\{C_R\Delta T - [(P_i + P_o)(V_o - V_i)]/2 + \int_{V_i}^{V_f} P_s(V)\, dV\right\}^{1/2} \quad (8)$$

To a large extent, Eq. (8) is indicative of the effects of peak shock pressure on the residual mechanical properties, viz. yield strength, ultimate tensile strength, hardness, ductility, etc. However these effects occur because of pressure-induced microstructural changes. Equation (8) is a modified version of Grace's[23] expression.

II. PERMANENT CHANGES: RESIDUAL MICROSTRUCTURE - MECHANICAL PROPERTY RELATIONSHIPS

This section will deal exclusively with shock waves since this is the regime for which substantial information is available

in the literature. The strain rates in the range $1 - 10^6 s^{-1}$ deserve greater attention and have not been explored in sufficient depth, from a metallurgical point of view. There is an almost complete lack of substructual characterization by transmission electron microscopy. An up-to-date collection of contributions with detailed information on the metallurgical effects of shock waves is the book edited by the authors[25].

Although transient effects are important in the generation and propagation of shock waves in metals and other materials, these effects are often difficult to monitor accurately, and are of little consequence with respect to their effect on the residual physical and mechanical properties of materials, which are dependent upon the more-or-less stable microstructures created in the shock front. Graham[26] has recently discussed transient phenomena in some detail, and we will not pursue this in any detail here because we will be more concerned with shock residual microstructures and properties which are of a much more practical consequence in evaluating the performance of explosively hardened, welded, formed, or consolidated materials.

It is well known that microstructures of all types have some influence on the physical and mechanical properties of materials. These include grain boundaries in polycrystalline materials, precipitates and other inclusions and dispersoids, and other types of point, line, planar, and volume defects. The passage of a shock wave through a metal can have three prominent effects; existing microstructure can be altered, new substructural features can be created, or both can occur simultaneously.

Alterations can include the annihilation of crystal defects through shock-induced annealing which can result by shock heating at very high peak pressures (60 GPa in steels, for example). These effects are almost without exception pressure dependent, and as a consequence both microstructure and related properties are quantitatively if not qualitatively related to the peak pressure, P.

Difficulties have been encountered in attempts to relate residual microstructural phenomena to residual mechanical properties through peak shock pressure because in many cases the shock wave was not accurately defined and errors occurred in measuring both the peak pressure and the stress conditions. In order to quantitatively or even qualitatively assess the metallurgical effects of shock waves in metals, it is necessary to accurately define the stress (or strain) state, the pressure, and pulse duration. This can be achieved by utilizing experimental arrangements similar to that shown schematically in Fig. 6(b), and described in detail in the previous chapter and elsewhere[25]. In such designs, the shock wave can be very accurately described as a compressive wave, and the tensile relief wave is eliminated from the experimental sandwich by spallation in the spall plate. Consequently, thin sheets of metal or alloy material can be subjected to plane compressive shock waves producing microstructures which can be directly observed by transmission electron microscopy.

A. Grain Size Effects

It is rare that grain size is altered with shock wave

passage in a metal or alloy except where a thermal transient promotes annealing or recrystallization and grain growth. However it has now been demonstrated that the grain size prior to shock deformation has a very significant influence on residual properties, particularly hardness and yield strength. These features are illustrted in Fig. 7 which shows a Hall-Petch type response for residual yield stress and hardness at various shock pressures:

$$\sigma = \sigma_0 + K D^{-1/2} \tag{9}$$

and

$$H = H_0 + K' D^{-1/2} \tag{10}$$

where K and K' are constants and D is the average grain size (grain diameter). The relationship between Eq. (9) and Eq. (8) is certainly obvious.

Moin and Murr[28], Greulich and Murr[29], Kestenbach and Meyers[30], Wongwiwat and Murr[31], and Murr[27] have discussed the effects of grain size on the development of microstructure and have shown that variations in grain size can have a significant effect on the production of deformation twins, martensitic transformation, and even dislocations.

B. Shock-Induced Microstructures

Dislocations are generated in the shock front without exception. If the wave profile has a shape shown ideally in Fig. 6(a), the dislocations generated will remain as a relatively stable microstructure behind the shock pulse as described in the

preceeding chapter, although some rearrangement, multiplication, or annihilation can occur in the relief portion of the pulse. As shown in Eq. (9), the generation of dislocations can be influenced by the grain size, but there is also an important effect of slip systems available and the ability of dislocations generated in the shock front to cross-slip, glide, or climb. While glide and climb may be influenced by temperature and other parameters, cross-slip will depend primarily on the stacking-fault free energy. This is particularly true in face-centered cubic metals where slip is restricted to the {111} planes, and dislocation motion is almost completely governed by the ability of dislocations to extend, forming partial dislocations separated by a region of stacking fault which increases with decreasing stacking-fault free energy.

Figure 8 illustrates these features for a number of common face-centered cubic metals and alloys with stacking-fault free energies noted[32], and shock loaded at a similar peak pressure and at a constant pulse duration utilizing the experimental design concept illustrated in Fig. 6(b). Figure 8 shows that at high stacking-fault free energies ($\geq$ 70 mJ/m^2) dislocations cannot extend appreciably and cross-slip is predominant. With sufficient time available in the shock pulse[33], this produces disloction arrays which form cell-like structures particularly prominent in shock-loaded nickel. As the stacking-fault free energy is reduced by alloying, cross-slip is discouraged or impossible, and dislocations form planar arrays which include extended stacking faults in the {111} planes. In many materials,

regular or periodic arrays of stacking faults can produce new phase regimes or twins. Indeed when intrinsic stacking faults form on every {111} plane, the region encompassed is a twin of the unfaulted region. During shock loading, these regions form irregularly, creating faulted twins or twin-faults. Figure 9 illustrates this phenomenon in type AISI 304 stainless steel subjected to explosively generated shock waves having various peak pressures indicated.

It is apparent from Fig. 9 that the microstructural "density" is increasing with increasing peak pressure. Indeed, as the number of dislocations or stacking faults increases, the volume fraction of deformation twin-faults increases, their size increases and their spacing decreases (the inter-twin spacing decreases). Similarly, in the case of high stacking-fault free energy face-centered cubic materials, increasing dislocation density with increasing peak shock pressure will cause an increase in the dislocation cell density, and this can only occur by decreasing the mean cell size or by increasing the number or density of dislocations composing the cell walls. This feature is illustrated in Fig. 10.

There are exceptions[34] to the rule of increase in flow stress with shock loading. Figure 11 shows a flow stress decrease found in RMI 38644 titanium alloy up to pressures of 10 GPa (100 Kbar). This decrease is due to a pressure-induced phase transformation; the alloy is in the metastable beta state; shock loading produces the reversion to the omega phase, which has a lower yield stress and UTS. At lower pressures the

transformation effect is more important than the one due to dislocations generated, resulting in an overall strength decrease.

It is apparent on comparing Figs. 9 and 10 that in addition to changes in dislocation density with shock pressure, other microstructural geometries or dimensions change. These changes will influence the residual mechanical properties as generally described by Ashby[35]:

$$\sigma = \sigma_0 + K(\lambda^G)^m \qquad (11)$$

where K is a constant which can be made similar or identical to that in Eq. (9), and λ^G is a wavelength equal to the spacing between specific phases or microstructural features. The specific nature of these regimes will determine the value of m, which will be equal to or less than 0.5 for grain boundaries, and increase for other, lower-energy interfaces, becoming unity for dislocation cells. In effect, gradients of plastic deformation are imposed by the microstructure, and λ^G can be regarded as the grain size, D, the dislocation cell size, d, or the inter-twin spacing, Δ. When microstructures become mixed, such as the intermixing of dislocation cells and deformation twins, they will each contribute to the resulting strengthening, and this can be illustrated by an equation of the form

$$\sigma = \sigma_0 + K\rho^{1/2} + K'V_c d^{-1} + K''V_T\Delta^{-1/2} + K_0 D^{-1/2} \qquad (12)$$

where the K's are associated constants, and V_c and V_T represent the approximate volume fractions of dislocation cells and deformation twin-faults respectively. Certainly Eq. (12) must be

regarded more as a qualitative guide than an empirically accurate description of microstructural strengthening, but a comparison of Eq. (12) with Eq. (9) will confirm the fact that peak pressure will have a profound effect upon both the residual microstructure and the associated physical and mechanical properties in shock-loaded metals and alloys.

Figures 12 and 13 illustrate the features implict in Eq. (12) for shock-loaded nickel where dislocation cell structures form as shown in Fig. 10 with increasing pressure of roughly 30 GPa, at which point deformation twin-faults occur with increasing frequency (and decreasing inter-twin spacing, Δ) at increasing peak shock pressure ($P > 30$ GPa).

Figure 14(a) summarizes the variations in residual hardness with peak shock pressure for a large number of metals and alloys. The peak pressures do not exceed the range of systematic microstructural change, and are below the range of higher pressures which produce shock-thermal effects by shock heating[11,20,21]. However Fig. 14(b) shows these effects for hardness changes at very high peak shock pressures, and Fig. 15 shows, by comparison with Fig. 9, the unique microstructural variations which occur in type AISI 304 stainless steel at very high pressures where shock heating effects are imposed upon the microstructural development. The sub-grain cell structures shown in Fig. 15 are to be recognized as distinct from the dislocation cell-type microstructures shown for shock-loaded nickel in Fig. 10.

The shock heating effects illustrated in Figs. 15 and 16

must be recognized to be very different from those frictional heating effects which are important in explosive compaction, inducing particle melting and melt-controlled consolidation. However, at sufficiently high pressures, the heat generated by the shock transient can contribute to these effects, and vice-versa.

Of particular significance from both a fundamental and applied point of view is the pressure-induced phase transformation undergone by iron and steel. At 13 GPa the BCC (α) phase transforms into the HCP(ε) phase. The kinetics of this transformation are rapid enough for it to be produced by the shock wave. This phase transformation has been studied in detail by many investigators (e.g., refs. 36 and 37). The high-pressure phase retransforms to α in the release (or rarefaction) part of the way, but profuse remnants of the transformation are left in the microstructure, they have been described by Stone et al[68] as "shear plates", and are somewhat similar to elongated sub-grains. This additional increase in defects reflects itself in a significant increase in hardness. Figure 16 shows the experimental results found for shock-loaded iron and low-carbon steel by Dieter[17], Zukas[16] and Stone et al[8]; they agree fairly well. At 13 GPa one has an increase in hardness of approximately HV 100 (from HV 250 to HV 350). Above this pressure there is no substantial gain in hardness; indeed, shock recovery effects discussed in the preceding paragraph start above 50 GPa. The microstructural changes produced by this phase transformation can be seen by optical microscopy. Figure 17 shows the change

introduced by the transformation. Deformation twins can be seen in Fig. 17(a), typical of a region shocked below 13 GPa. The dark regions that are highly etched are due to the transformation debris, in Fig. 17(b).

Figure 18 shows the deformation undergone by rapidly-solidified Mar M-200 powders during shock-wave consolidation[70]. The hardness is significantly increased by the passage of the shock wave: HV 400 to HV 720. In addition to shock-hardening perse, one has high strain-rate deformation at the external regions of the particles and heating due to friction between the particles. The dendritic structure produced by the RSP[42] process can be clearly seen in Fig. 18(a) and the deformation at the boundaries of the particles is reflected by the distortion of the dendritic pattern, that was initially regular. The clear islands between particles represent melted (or recrystallized) regions; they are highly localized, and does not affect the regions adjacent to it because of the high cooling rates.

Figure 18(b) shows the deformation substructure in the center of one of the shock-consolidated Mar M-200 particles. It is characteristic of shock loading. The dislocations are organized in planar arrays and their density is extremely high. This high dislocation density is responsible for the significant hardness increase in dynamic consolidation. The substructure close to the interfaces where bonding occurred is different, because the uniaxial strain state condition required for shock waves is not obeyed.

C. Shock Deformation versus Conventional Deformation (Cold Reduction)

Although it is unnecessary to draw extensive comparisons between shock loading and more conventional deformation (characterized by more complex stress states and lower strain rates), it must be recognized that shock loading is unique as a result of the significant hardening and strengthening which arises from shock wave propagation, while the residual strains are small or even negligible. Although there are significant differences in a cold-reduction mode of deformation as compared to well-controlled shock compression, it is of interest to note that the corresponding microstructures attendant to the production of specific mechanical responses are normally produced in shock deformation at significantly lower true strains when compared to the through-thickness true strains in cold reduction. This feature is illustrated in the experimental data shown plotted for comparison in Fig. 19. It is particularly significant to note that, as implicit in Fig. 13, there is a particular strength (yield stress) or hardness associated with a particular dislocation cell size in nickel, and this is achieved at significantly lower and even negligible residual strains in shock deformation as compared to other forms of deformation. This is certainly one of the very practical and important aspects of shock hardening. Since the residual strain is very small, one would expect an anisotropy of strengthening; this is indeed observed. One would expect that no specific texture is introduced by the shock wave, in contrast to most conventional

deformation processes. Indeed[71], Trueb[72], and Dhere et al[73] have found no change in texture upon shock loading copper, nickel and aluminum, respectively.

D. Effects of Shock Pulse Duration in Shock Loading

Murr and Kuhlmann-Wilsdorf[33] have discussed the fact that while the quantitative features of the microstructure, particularly dislocation density, are controlled almost exclusively by the peak pressure, the qualitative features such as the definition of dislocation cell structures, dislocation cell wall definition, and the like, depend upon the time the pulse is applied, i.e. the shock pulse duration (Δt in Fig. 6(a)). These features have recently been reviewed in considerable detail[35], and will not be pursued here. However it must be pointed out that as result of these effects, there is usually no significant variation in mechanical properties such as yield strength and especially hardness over a fairly wide range of shock pulse durations above about 1 μs. These effects are summarized in the hardness data plotted in Fig. 20.

It is important to realize that the pulse durations noted in Fig. 20 and in the other figure descriptions presented in this chapter were carefully controlled by adjusting the driver-plate thickness in experiments characterized explicitely by Fig. 6(b). In these experiments, the shock pulse duration, Δt, can be fairly accurately determined from[37,38].

$$\Delta t \simeq 2\, h_d/U_s, \qquad (U_s = \text{shock velocity}) \tag{13}$$

where at high pressures (> 5 GPa) we can write

$$\Delta t \cong 2h_d U_p \rho_o / P \qquad (U_p = \text{particle velocity}) \qquad (14)$$

It can be observed, somewhat qualitatively, that in order to maintain a constant shock pulse duration with increasing peak shock pressure, the flyer-plate thickness must be increased.

E. Effects of Point Defects, Precipitates, and Other Second-Phase Particles

Because of the rapid movement of dislocations generated in the shock front[39], intersections forming jogs favor vacancy formation in large quantities. These features were demonstrated experimentally by Kressel and Brown[40], and Murr, et al[42] have also shown that vacancies and vacancy clusters make a direct contribution to residual shock hardening. In addition, vacancies present in shock-loaded metals contribute significantly to thermal recovery phenomena, and hardness recovery has been demonstrated to occur even catastrophically for shock-hardened metals and alloys[38]. A high concentration of point defects, particularly vacancies, is therefore a somewhat unique feature of the residual shock microstructure in explosively loaded metals and alloys.

Although it might be expected that shock-induced point defects might lead to the formation of precipitates or other similar inclusions, evidence for this phenomenon is meager[39,43]. On the other hand, precipitates and other second-phase particles (both coherent and non-coherent) can have a profound effect on shock-loaded metals and alloys. Initially of course particle distributions strengthen and harden a matrix by providing for

deformation gradients having a wavelength equal to the mean particle (or interparticle) spacing [Eq.(11)]. Following shock loading, dislocations generated in the shock front add additional, significant strength which can be described by an equation of the form of Eq. (12). Furthermore, such particles or precipitates can not only block the initial (shock) formation of crystal defects[44], but can also block their annihilation by shock heating or post-shock annealing or heat treatment. This feature is illustrated in Fig. 21. Figure 21(a) also illustrates the very rapid and even catastrophic recovery alluded to above. However, this phenomenon is not universal, and Inconel 718 shock loaded to a pressure of 51 GPa and cold rolled (20 pct reduction in the thickness) exhibited about the same recovery response, when subjected to isochronal anneals (1 hour). This is evidenced by Fig. 22. The shocked and rolled conditions show the same hardness decrease.

Because of the density differences imposed by precipitates and other inclusions, impedance mismatch can lead to local spallation at the particle-matrix interface or other aberrations in the wave profile can occur through the mechanism proposed by Meyers[46] for the production of a wavy-wave in a polycrystalline metal or alloy. Moreover, Murr and Foltz[47] have demonstrated experimentally that coherent precipitates can become non-coherent following shock loading at sufficiently high peak pressures, and that with the loss of coherency, the precipitates become engulfed by dislocations. It is also certain that many precipitates and other inclusions serve as dislocation sources during the shock-

loading of metals and alloys which contain them, when they have different compressibilities. Geometrically - necessary dislocations are generated around the interface to accommodate the strains.

III. RESPONSE OF METALS TO THERMOMECHANICAL SHOCK TREATMENT

In the foregoing treatment in Section II above, we have attempted to provide an overview of structure - property relationships (mainly simple mechanical relationships), associated with explosively shock-deformed metals and alloys. It should be apparent from this treatment that there are some unique features of shock-induced microstructures when compared with more conventional deformation microstructures, and there are correspondingly unique mechanical properties. Figure 22 is a particularly convincing example of the unique features of shock hardening. Overall, the metallurgical effects of shock wave propagation are not generally unlike those of other deformation modes where microstructures are created which evoke particular physical and mechanical responses.

Cooperative strengthening effects between mechanical and thermal treatments can be achieved by thermomechanical processing (TMP) or thermomechanical treatments (TMT). In such treatments, microstructures created by mechanical (deformation) treatment can be altered through thermal (annealing, quenching, etc.) treatments, and vice-versa. Central to the effective utilization of this concept is of course the ability to control both composition and microstructure, and to carefully monitor these

changes in consonance with alterations in specific properties.

The phase transformations that deformation and heat treatments can create in steels make them particularly amenable to TMT, and there are numerous examples of such applications[48,49]. There are, by comparison, currently few applications of shock TMT or thermomechanical shock treatment (TMST), although the concept of TMST has been discussed in a recent review by Meyers and Orava[50].

The results shown in Fig. 22 suggest that the creation of second phases by aging and other treatments followed by shock loading, or similar TMST schedules could provide unique metallurgical properties, and indeed this has been demonstrated for example in nickel-base superalloys such as Udimet 700[51] and Inconel 718[45,52]. Figure 23 shows constant load creep curves for Udimet 700 and Inconel 718 at 649°C. The benefits arise mainly by the development of a high volume fraction of finely-dispersed precipitates (γ'), and a finely-dispersed, thermally-stabilized dislocation substructure. Aging treatments of 100 h at 789°C gave rise to extensive δ formation along the {111} planes in the Inconel 718 matrix, while it was only occassionally observed in the cold-rolled material and absent in the undeformed material for the same heat treatment. Some of these effects arise from the high vacancy concentrations associated with the shock deformation as briefly described above and in the previous chapter. Some evidence for the effect of vacancies on precipitation is also suggested in the work by Greenhut, et al[53] involving an aluminum alloy.

Because of the ability of high-pressure shock waves to produce particular microstructural phenomena, it is of course futile to assess the shock TMP response of a specific material on the basis of room temperature tensile properties alone, because, as shown in Fig. 23, there are frequently very particular metallurgical effects which are recognized only under very specific conditions. Certainly Fig. 23 illustrates a condition where shock TMP is superior to conventional TMP.

A. Shock-Mechanical Treatment, Stress-Cycling and Repeated Shock Loading

As we noted previously (Fig. 14(b)), most metals and alloys, depending upon their particular melting points and other properties, will begin to heat up appreciably both during and after shock wave propagation at sufficiently high peak pressure. This limitation can be circumvented to some extent by conventionally deforming a material prior to shock deformation, by shocking repeatedly, or by some other stress-cycling involving shock deformation. In any of these treatments, which may not always specifically involve TMP (although many processes begin with some conventional annealing treatment), the initial deformation process (either conventional or shock loading) creates a microstructure which in effect work hardens the material. The second deformation process then involves an interaction with this microstructure creating modifications which can lead to an increase (or decrease) in defect density, a change in the type of defect, or both.

Staudhammer and Murr[54] have described experiments involving schedules of cold-reduction and shock cycling of stainless steels which clearly illustrate a sensitivity of residual microhardness of sheet samples to the particular deformation schedules. This is shown in Fig. 24 for deformed type 304 stainless steel. Although it was originally demonstrated by Staudhammer and Murr[54] that the relative amounts of residual α' martensite changed with the deformation cycling, it has only recently been shown that this feature, along with the hardness responses shown in Fig. 24 probably occur by one deformation mode (cold reduction) being more conducive to martensite formation because nucleation and growth is retarded by adiabatic heating associated with shock loading at room temperature[55]. This occurs because deformation of AISI 304 stainless steel produces twin-fault intersections which increase with increasing deformation. α' martensite nucleates at these intersections as originally described by Olson and Cohen[56], but at high strain rates, adiabatic heating suppresses this process. Consequently, shock loading can produce additional intersections but not necessarily additional martensite, whereas cold reduction will cause more efficient transformation at the intersections formed during deformation.

When the number of such shock-induced intersections in AISI 304 stainless steel is increased substantially, large amounts of α' martensite can form irregular morphologies by coalescence, and this can be achieved by repeated shock loading as described by Kazmi and Murr[57]. However, while dramatic changes in α' martensite content are observed as shown in Fig. 24, there is

very little difference in net, residual yield stress increase, while the hardness increment increases substantially with the production of large volume fractions of martensite. This is illustrated in Fig. 25 for AISI 304 stainless steel and similar results were observed on doubly-shocked Inconel 718 in earlier work by Meyers[52]. However, Meyers[52] concluded from TMP experiments involving doubly shocked Inconel 718 that multiple shocking will yield attendant strength improvements. This feature is demonstrated in Fig. 26, but it is imperative, as pointed out earlier, to recognize that specific conditions (residual mechanical properties) may not always be able to provide a generalized concept of the repeated shock loading effects. The response may be very different at different shock mechanical or TMP treatments, etc.

It should also be recognized, as is perhaps implicit in Fig. 25, that repeated shock loading is not an additive process in terms of residual mechanical properties. That is, shock loading twice at a constant pressure, P, is not generally equivalent to shock loading once at twice the pressure, i.e. $2\,P_1 \neq P_1 + P_1$, etc. This occurs because each wave establishes a different kind of interaction with the structure of the material.In the case of the 304 stainless steel in Fig. 25, the second event does not produce much additional martensite and the twin-faults as shown in Fig. 25(a) probably impede additional twin-fault development, however after the third shock event, the change in microstructure causes an attendant change in hardness, while the yield stress becomes saturated. In the case of nickel, the formation of dislocation

cells as shown in Fig. 10(a) typifies the first shock event. Successive events simply decrease the cell size and increase the dislocation density. The second event causes a marked reduction in the dislocation size as well as a densification of the cell wall dislocation density. The third event, while decreasing the dislocation cell size and increasing the dislocation density, does not cause a concomitant increase in the hardness and yield stress.

B. Microstructural Stability and Thermal Stabilization of Substructure

There is some evidence that certain shock-induced microstructures are mechanically unstable[50,59]. This can arise because dislocation arrays can be easily re-arranged when deformed after shock loading. This is particularly true in metals and alloys which, because of their stacking-fault energy (FCC materials) or available slip systems (or multi-slip systems) (BCC materials), form poorly-structured dislocation cells or other tangled arrays of dislocations (see Figs. 8 and 10). Indeed such work-softening, which results when materials with unstable microstructures are deformed in uniaxial tension, has been observed in nickel[59] (which forms dislocation cell structures in response to shock loading as shown in Figs. 8 and 10), and in a magnetic ingot iron [which forms dislocation cell-like tangles similar to those shown in Fig. 8(c)]. This is apparently true only in the case where the microstructures are poorly developed.

In addition, work softening can be reduced or eliminated by thermal stabilization of the microstructure. This treatment

simply involves an anneal following shock loading which allows the dislocations composing the microstructure to re-arrange themselves into a more stable (equilibrium) sub-structure. As illustrated in Fig. 27, work softening can be eliminated with little loss in yield strength by annealing shock loaded metals under appropriate conditions. Such thermal stabilization treatments do not, strictly speaking, qualify as being described as thermomechanical processing. They are really mechanical - thermal treatments (MTT), and as such are strictly a substructural control process. Such treatments can be useful in stabilizing other microstructures because they can affect impurity segregation, and solubility, and as a consequence alter impurity pinning effects on dislocations and other recovery microstructures. The general subject of mechanical-thermal treatments of microstructures has been treated in a review by McElroy and Szkopiak[60]. The shock-loaded nickel specimen of Fig. 25 (25 GPa, 2μs) exhibits a significant work-hardening rate after being annealed at 400°C for one hour, without significant loss in the yield stress.

On a substructural level, work softening can be explained by the replacement of the unstable substructure generated by shock loading by the one stable under the imposed conditions. Longo and Reed-Hill[62] found work softening in a number of high S.F.E. FCC alloys and attributed it to dynamic recovery during the tensile test. The same explanation applies to the case of shock loading, as evidenced by Fig. 28. This TEM specimen was cut from the region in the tensile specimen where work softening was

occurring (neck region). An elongated cell many times larger than the shock-induced cells is clearly seen; its walls exhibit a much higher dislocation density than the original walls. It seems that the applied stress during tensile testing promotes the movement of the existing dislocations into these new arrays, rather than the generation of new dislocations (as in the case of conventional work hardening). So, the process of work softening is associated with dislocation cross-slip, annihilation, or climb, but no dislocation multiplication. Indeed, Kuhlmann-Wilsdorf and Laird[63] have analyzed similar elongated cells in fatigue. They are of "near-minimum energy configurations of the stored dislocation content". Fatigue tends to generate dislocation configurations that are more stable than conventional tensile testing. Pre-strained material (by uniaxial tensile extension, for instance) can undergo cyclic softening by fatigue, which is accompanied by cell formation. This lends support for the explanation advanced by Meyers[5] and Hsu[61] for work softening.

IV. SUMMARY AND CONCLUSIONS

Beginning with a development of a simple expression for the influence of shock or pressure waves on the residual yield strength of metals and alloys [Eq. (16)], we have demonstrated experimentally observed microstructural development in response to uniaxial shock loading, and the corresponding influence on residual hardness and strength of shock-loaded metals and alloys. We have, to a large extent, limited our attention to an exposition of the conditions which are likely to be encountered,

perhaps in a more complex and synergistic way, in explosive compaction and consolidation of powders. However, this development is particularly applicable to the response of metals and alloys in explosive fabrication hardening, and other forms of explosive metal working.

We have shown in Section II, that shock-induced microstructures, while frequently similar to those characteristic of more conventional deformation, are sometimes unique, and form at significantly lower equivalent or true strains than in conventional deformation. However, as we demonstrate in Section III, certain instabilities can occur for particular shock-induced microstructures. While these microstructures can be modified by heat treatment, there can be significant mechanical property consequences. Indeed, shock thermomechanical treatments or processing can also have significant effects on the residual mechanical properties of shock-loaded metals and alloys. More importantly, these effects can be very specific to a particular response such as creep life, fatigue life, tensile strength, ductility, etc. Furthermore, shock-wave interactions with existing microstructure as in the case of the repeated shock loading of a particular material or solid volume can also result in substructures and related mechanical properties which are unique to that particular mode of deformation.

It must be recognized that, in the case of explosive consolidation of metal powders for example, that the shock wave can produce effects within individual particle volumes which have been described here in terms of metallurgical effects. These

effects most certainly must include thermal effects not only associated with the shock transient heating, but also with the frictional contact which characterizes the compaction and consolidation process and on the high-velocity deformation taking place in the external layers of the particles. As a consequence, the properties of explosively consolidated products will depend to a large extent upon this process synergism. To some extent, these consolidated masses will function as complex composites of phases having different stoichiometry, crystallography, and microstructure which can be altered by altering the shock or pressure-wave parameters (peak pressure and pulse duration for example).

ACKNOWLEDGMENTS

Many of the observations presented here, and the research described in connection with our own explosive shock loading programs over the past decade and more, have been supported by the Department of Energy through contracts with Sandia Laboratories (L.E.M.), and by the National Science Foundation and the Instituto Militar de Engenharia (M.A.M.). Portions of this work were also supported by the Research and Development Division of New Mexico Tech.

REFERENCES

1. Argon, A.S., ed., "Constitutive Equations in Plasticity", MIT Press, Cambridge, Mass, 1975.
2. Hart, E.W., Trans. A.S.M.E., 98 (1976) 193.
3. Swearengen, J.C., Rohde, R.W., and Hicks, D.L., Acta Met., 24 (1976) 969.
4. Campbell, J.D., Dynamic Plasticity of Metals, Springer-Verlag, Vienna Austria, 1972.
5. Maiden, C.J., and Green, S.J., Trans. A.S.M.E., J. Appl. Mech., 33 (1966) 496.
6. Lindholm, U.S., in "Techniques of Metals Research", Vol. 5, ed. R.F. Bunshah, Interscience, NY, 1974, p. 199.
7. Lindholm, U.S., and Yearley, J. Exptl. Mech. 7 (1967) 1.
8. Culver, R.S., Exptl. Mech., 12 (1972).
9. Culver, R.S., in "Metallurgical Effects at High Strain Rates", Eds. R.W. Rohde, B.M. Butcher, J.R. Holland, and C.H. Karnes, Plenum, NY, 1973, p. 519.
10. Warnes, R.H., Duffey, T.A. Karpp, R.R., and Carden, A.E., in "Shock Waves and High-Rate Phenomena in Metals: Concepts and Applications", eds. M.A. Meyers and L.E. Murr, Plenum, NY, 1981, p. 23.
11. Kolsky, H., Proc. Phys. Soc. (London) B, 62 (1949) 676.
12. Wasley, R.J., Stress Wave Propagation in Solids, M. Dekker, New York, 1973.

13. Orava, R.N., and Wittman, R.H., in "Advances in Deformation Processing", eds. V. Weiss and J. Burke, Plenum, NY, 1978.

14. Orava, R.N., in Proceedings of the First International Conference of the Center for High Energy Forming, ed. A.A. Ezra, U. of Denver, Colo., 1978, p. 7.5.1.

15. Zener, C., and Hollomon, J.H., J. Appl. Phys., 15 (1944) 22.

16. Olson, G.B., Mescall, J.F., and Azrin, M., in Shock Waves and High-Strain-Rate Phenomena in Metals: Concept and Applications, eds. M.A. Meyers and L.E. Murr, Plenum, NY, 1981, Chapter 14, p. 221.

17. Shockey, D.A., and Erlich, D.C. source cited in ref. 16, Chapter 15, p. 249.

18. Doraivelu, S.M., Gopinathan, V., and Venkatesh, V.C., source cited in Ref. 16, Chapter 16, p. 263.

19. Rogers, H.C., and Shastry, C.V., sources cited in Ref. 16, Chapter 18, p. 285.

20. Moss, G.L., source cited in Ref. 16, Chapter 19, p. 299.

21. National Materials Advisory Board, Materials Response to Ultra-High Loading Rates. Report NMAB 356, 1980, Chapter 8.

22. Walsh, J.M., and Christian, R.H., Phys. Rev. 97 (1955), 1544.

23. Grace, F.I., J.Appl. Phys., 40 (1969) 2649.

24. Hsu, C.Y., Hsu, K.C., Murr, L.E., and Meyers, M.A., source cited in Ref. 16, p. 433.

25. Meyers, M.A., and Murr, L.E. (eds.) Shock Waves and High-Strain-Rate Phenomena in Metals: Concepts and Applications, 1981, Plenum Press, New York.

26. Graham, R.A., in Shock Waves and High-Strain-Rate Phenomena in Metals: Concepts and Applications, Chap. 23, Meyers, M.A. and Murr, L.E. (eds) 1981, Plenum Press, New York.

27. Murr, L.E., in Shock Waves and High-Strain Rate Phenomena in Metals: Concepts and Applications, Chap. 37, Meyers, M.A., and Murr, L.E. (eds.) 1981, Plenum Press, New York.

28. Moin, E., and Murr, L.E., Mater. Sci. Engr., 37 (1979), 249.

29. Greulich, F., and Murr, L.E., Mater. Sci. Engr., 39 (1979), 81.

30. Kestenbach, H.-J., and Meyers, M.A., Met. Trans., 7A (1976).

31. Wongwiwat, K., and Murr, L.E., Mater. Sci., Engr., 35 (1978), 273.

32. Murr, L.E., Interfacial Phenomena in Metals and Alloys, 1975, Addison-Wesley, Reading, Mass.

33. Murr, L.E., and Kuhlmann-Wilsdorf, D., Acta Met., 26 (1978), 847.

34. Rack, H.J., Met. Trans., 7A (1976), 1571.

35. Ashby, M.F., Phil. Mag., 21 (1970), 399.

36. Murr, L.E., in Shock Waves and High-Strain Rate Phenomena in Metals: Concepts and Applications, Chap. 42, Meyers, M.A. and Murr, L.E. (eds.), 1981, Plenum Press, New York.

37. McQueen, R.G., and Marsh, S.P., J. Appl. Phys., 31 (1960), 1253.

38. Murr, L.E., and Rose, M.F., Phil Mag., 18 (1968), 281.

39. Meyers, M.A., and Murr, L.E., in Shock Waves and High-Strain-Rate Phenomena in Metals: Concepts and Applications, Chap. 30, Meyers, M.A., and Murr, L.E., (eds.), 1981, Plenum Press, New York.

40. Kressel, H., and Brown, N., Appl. Phys., 38 (1967), 1618.

41. Murr, L.E., Inal, O.T., and Morales, A.A., Acta Met., 24 (1976), 261.

42. Murr, L.E., Inal, O.T., and Morales, A.A., Appl. Letters, 28 (1976) 432.

43. Stein, C., Scripta Met., 9 (1975), 67.

44. Murr, L.E., Vydyanath, H.R., and Foltz, J.V., Met. Trans., Al (1970), 3215.

45. Meyers, M.A., "Thermomechanical Processing of a Nickel-Base Superalloy by Cold-Rolling and Shock-Wave Deformation", Ph.D. Dissertation, 1974, Univ. of Denver, Denver, Colorado.

46. Meyers, M.A., Mater. Sci. Engr., 30 (1977), 99.

47. Murr, L.E., and Foltz, J.V., J. Appl. Phys., 40 (1969), - 3796.

48. Delaey, L., Zeitschriff Metallk., 63 (1972), 531.

49. Zackay, V.F., Mater. Sci. Engr., 25 (1976), 247.

50. Meyers, M.A., and Orava, R.N., in Shock Waves and High-Strain-Rate Phenomena in Metals: Concepts and Applications, Chap. 45, Meyers, M.A., and Murr, L.E. (eds.), 1981, PLenum Press, New York.

51. Orava, R.N., Mater. Sci. Engr., 11 (1973), 177.

52. Meyers, M.A., and Orava, R.N., Met. Trans., 7A (1976), 179.

53. Greenhut, V.A., Chen, M.G., Banks R., and Golaski, S., "Long-Range Diffusion of Vacancies and Substitutional Atoms during High-Strain-Rate Deformation of Aluminum Alloys", Proc. ICM II, Boston, Mass., 1975.

54. Staudhammer, K.P. and Murr, L.E., Mater. Sci. Engr., 44 (1980), 97.

55. Staudhammer, K.P., Frantz, C.E., Hecker, S.S., and Murr, L.E., in Shock Waves and High-Strain-Rate Phenomena in Metals: Concepts and Applications, Chap. 7, Meyers, M.A. and Murr, L.E. (eds.), 1981, Plenum Press, New York.

56. Olson, G.B., and Cohen, M., J. Less Common Metals, 28 (1972), 107.

57. Kazmi, B., and Murr, L.E., in Shock Waves and High-Strain Rate Phenomena in Metals: Concepts and Applications, Chap. 41, Meyers, M.A., and Murr, L.E. (eds.), Plenum Press, New York.

58. Staudhammer, K.P., "Effect of Shock Stress Amplitude, Shock Stress Duration, and Prior Deformation on the Residual Microstructure of Explosively Deformed Stainless Steels", Ph.D. Dissertation, 1975, New Mexico Institute of Mining and Technology, Socorro, New Mexico 87801.

59. Meyers, M.A., Met. Trans. , 8A (1977), 1581.

60. McElroy, R.J., and Szkopiak, F.C., Intl. Metall. Reviews, 17 (1972), 174.

61. Hsu, K.C., M. Sc. Thesis, 1981, New Mexico Institute of Mining and Technology, Socorro, New Mexico 87801.

62. Longo, W.P., and Reed-Hill, R.E., Metallography, 4 (1974), 181.

63. Kuhlmann-Wilsdorf, D., and Laird, C., Mater. Sci. Eng., 27 (1977), 137.

64. Duvall, G.E., and Graham, R.A., Reviews of Modern Phys., 49 (1977) 523.

65. Barkers, L., and Hollenbach, R.E., JAP, 45 (1974) 4872.

66. Zukas, E.G., Metals Eng. Quart., 6 (1966) 1, May.

67. Dieter, G.E., in Response of Metals to High Velocity Deformation, Shewmon, P.G., and Zackay, V.F., (eds.) Interscience, New York, 1961, p. 419.

68. Stone, G.A., Orava, R.N., Gray, G.T. and Pelton, A.R., "An Investigation of the Influence of Shock-Wave Profile on the Mechanical and Thermal Responses of Polycryustalline Iron", U.S. Army Research Office Final Report, Grant No. DAAG29-76-G-0180, September 1978, Report No. SMT-1-78.

69. Meyers, M.A., Sarzeto, C. and Hsu, C.Y., Met. Trans., 11A (1980) 1737.

70. Gupta, B.B., Meyers, M.A., and Murr, L.E., Met. Trans., submitted for publication (1981).

71. Higgins, G.T., Met. Trans., 2 (1971) 1277.

72. Trueb, L.F., JAP, 40 (1967) 2976.

73. Dhere, A.G., Kestenbach, H.-J., and Meyers, M.A., submitted for publication (1981).

FIGURE CAPTIONS

Fig. 1. Stress-strain, strain-rate plot for mild steel (From Ref. 4).

Fig. 2. Effect of strain rate on the compressive strength of 6061-T6 aluminum (From Ref. 5).

Fig. 3. Range of Explosive Fabrication processes (From Ref. 13).

Fig. 4. Effect of forming velocity on the maximum uniform strain during the explosive bulging of domes (From Ref. 13).

Fig. 5. Adiabtic shear band revealed by optical micrograph of steel. Tip of shear fracture preceded by shear zone (From Pearson and Finnegan in source cited in Ref. 10, p. 205).

Fig. 6. (a) Idealized view of a shock pulse traveling through a solid metal. The pulse duration is denoted Δt.

(b) Schematic view of an arrangement for shock loading sheet materials with plane compression waves, of known peak pressure.

Fig. 7. Effect of initial grain size on the residual yield stress (a) and hardness (b) of shock-loaded nickel and stainless steel (From data in Ref. 27).

Fig. 8. Examples of shock-induced microstructures in face-centered cubic metals having a range of stacking-fault free energies shown. (a) Ni(15 GPa), (b) Cu (15 GPa), (c) Fe-34% Ni(10 GPa), (d) $Ni_{80}Cr_{20}$(8 GPa)

Fig. 14. (a) Summary of shock strengthening (shock hardening) in a variety of metals and alloys (2 μs shock pulse duration) variations with grain sizes, are shown by error bars. (From Ref. 27).
(b) Hardness versus high shock pressure for nickel and type 304 stainless steel. Error bars correspond to variations in grain size (From Murr[27]).

Fig. 15. High-pressure (120 GPa) sub-grain microstructure in 304 stainless steel which results in large part by shock-thermal effects (compare with twin-fault microstructures shown in Fig. 9).

Fig. 16. Effect of shock-hardening pressure on the hardness of iron and steel (Adapted from Ref. 28).

Fig. 17. Optical micrographs of AISI 1008 steel shock loaded below (a), and above (b) 13 GPa. The transformation debris can be clearly seen in (b) (from Ref. 69).

Fig. 18. Shock-consolidated MAR M-200 superalloy (courtesy of B.B. Gupta). (a) TEM image from a region in (a) showing planar dislocation in arrays (b).

Fig. 19. Reciprocal dislocation cell size versus true strain for shock-loaded and cold-roll reduced nickel sheet. (Shock loading data from Ref. 27; cold reduction data courtesy of Dana Rohr, Los Alamos National Laboratory).

Fig. 20. Residual hardness (H) versus shock pulse duration (Δt) for a number of metals and alloys over a range

of peak pressures. The initial grain sizes (D) are indicated. (From Murr[36]).

Fig. 21. Comparison of hardness and recovery in shock-loaded $Ni_{80}Cr_{20}$ and TD-Ni Cr (the same alloy with 2 volume percent ThO_2 included as a dispersed particle distribution) for a constant annealing time of 1 h.

Fig. 22. Isochronal (1 hour) curves for undeformed, rolled (20% reduction) and shocked (52 GPa) Inconel 718 superalloy having been pre-aged at 1400°F/ 4 hours (From Ref. 45).

Fig. 23. Constant-load creep curves. (a) Udimet 700 at 649°C; TMP schedule: 1177 C, 4 h + cold work + 843 °, 24 h + 760°C, 16 h; σ = 0.8 GPa. (b) Inconel 718 at 649°C; shocked and rolled: 954°C, 1h + 704°C, 4 h + cold work + 677°C, 8 h F.C. to 621°C, total 18 h; undeformed, σ = 0.8 GPa.

Fig. 24. Residual hardness (H) versus shock pressure (P) for 304 stainless steel sheets subjected to deformation schedules shown: curve A is the annealed sheet with no deformation prior to or after shock loading; curve B; shocked + 15% cold reduction by rolling; curve C; shock loading; curve E: 15% cold reduction + shock loading 15% cold reduction, curve F: 30% cold reduction + shock loading. (Data from Ref. 36 and 40).

Fig. 25. Production of α' martensite by repeated shock loading of 304 stainless steel. (a) single shock event: 15 GPa

2 μs; (b) event in (a) repeated three times (shock loading three times at 15 GPa, 2 μs). The volume fraction of α' martensite in (a) is about 2% while in (b) it is 26%.

Fig. 26. Residual hardness increase, ΔH, and yield stress increase, $\Delta\sigma$, after repeated shock loading of nickel and 304 stainless steel (304 SS). The original, unshocked hardnesses were 1.8 and 1.0 GPa for stainless steel and nickel respectively. The increment is taken as the hardness before and after each event: $\Delta H = H_f - H_o$. The original, unshocked yield stresses were 0.25 and 0.14 GPa for the stainless steel and nickel respectively. The increment is taken as the 0.2% offset yield stress before and after each event; $\Delta\sigma = \sigma_f - \sigma_o$. Each shock event was characterized by a peak shock pressure of 15 GPa at 2 μs duration (data from Ref. 57).

Fig. 27. Elimination of work-softening in shock-loaded nickel (25 GPa; 2 μs) by thermal stabilization of the substructure (from Ref. 61).

Fig. 28. Dislocation substructure generated by conventional deformation of shock-loaded nickel (25 GPa, 2 μs) in a tensile test. The elongated cells are associated with work softening.

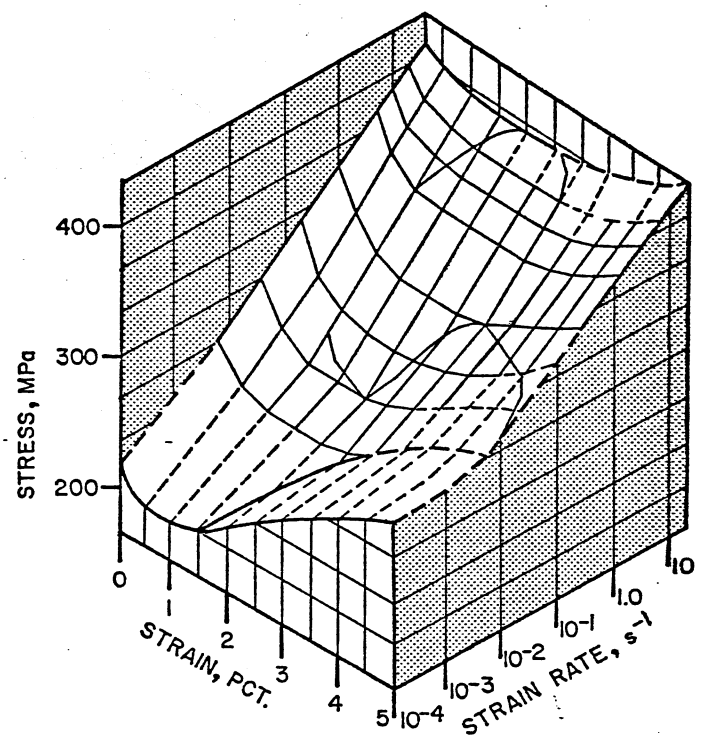

FIG. 1
MURR & MEYERS
CHAP. 3

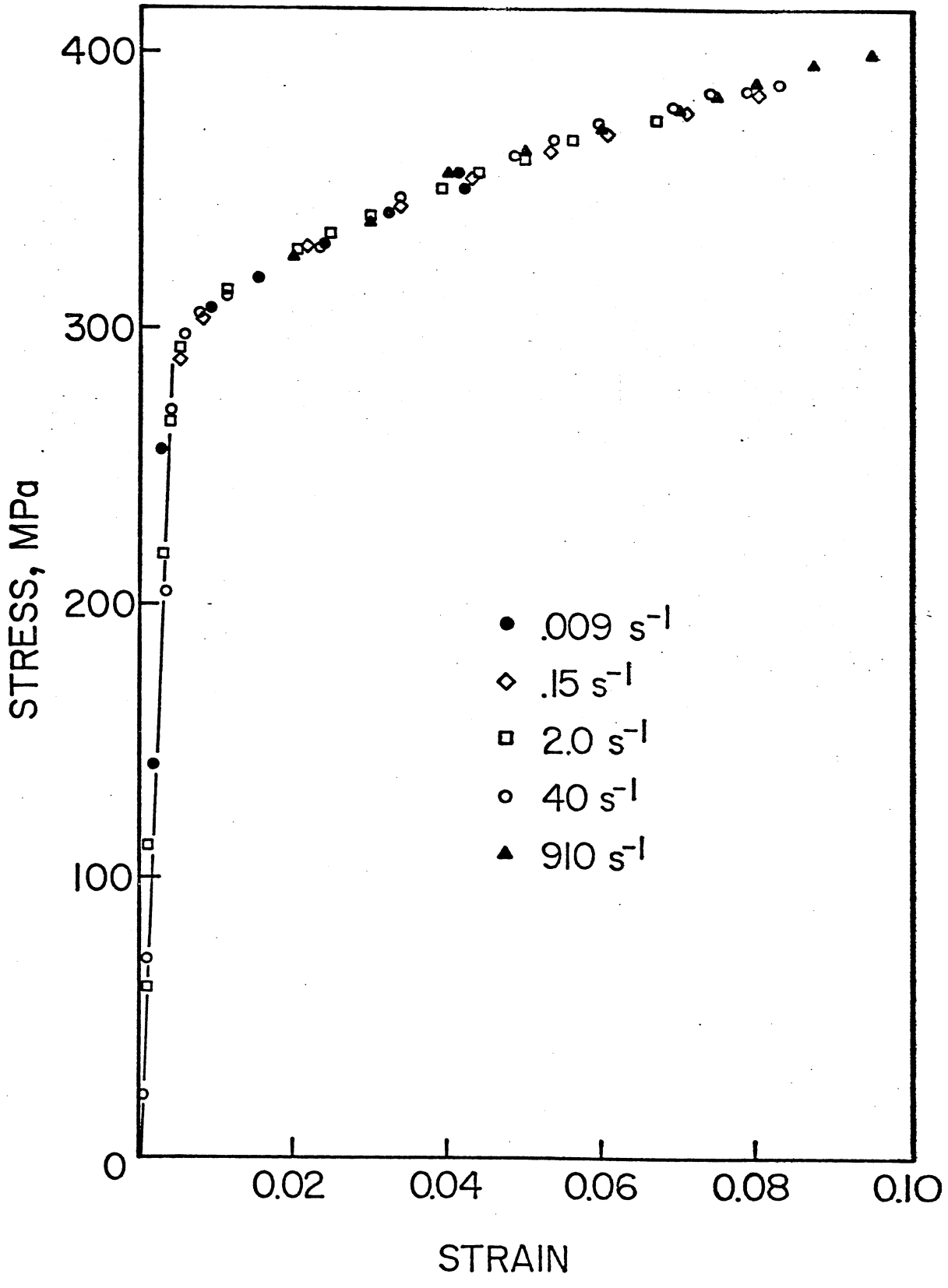

FIG. 2
MURR & MC-CLEAN

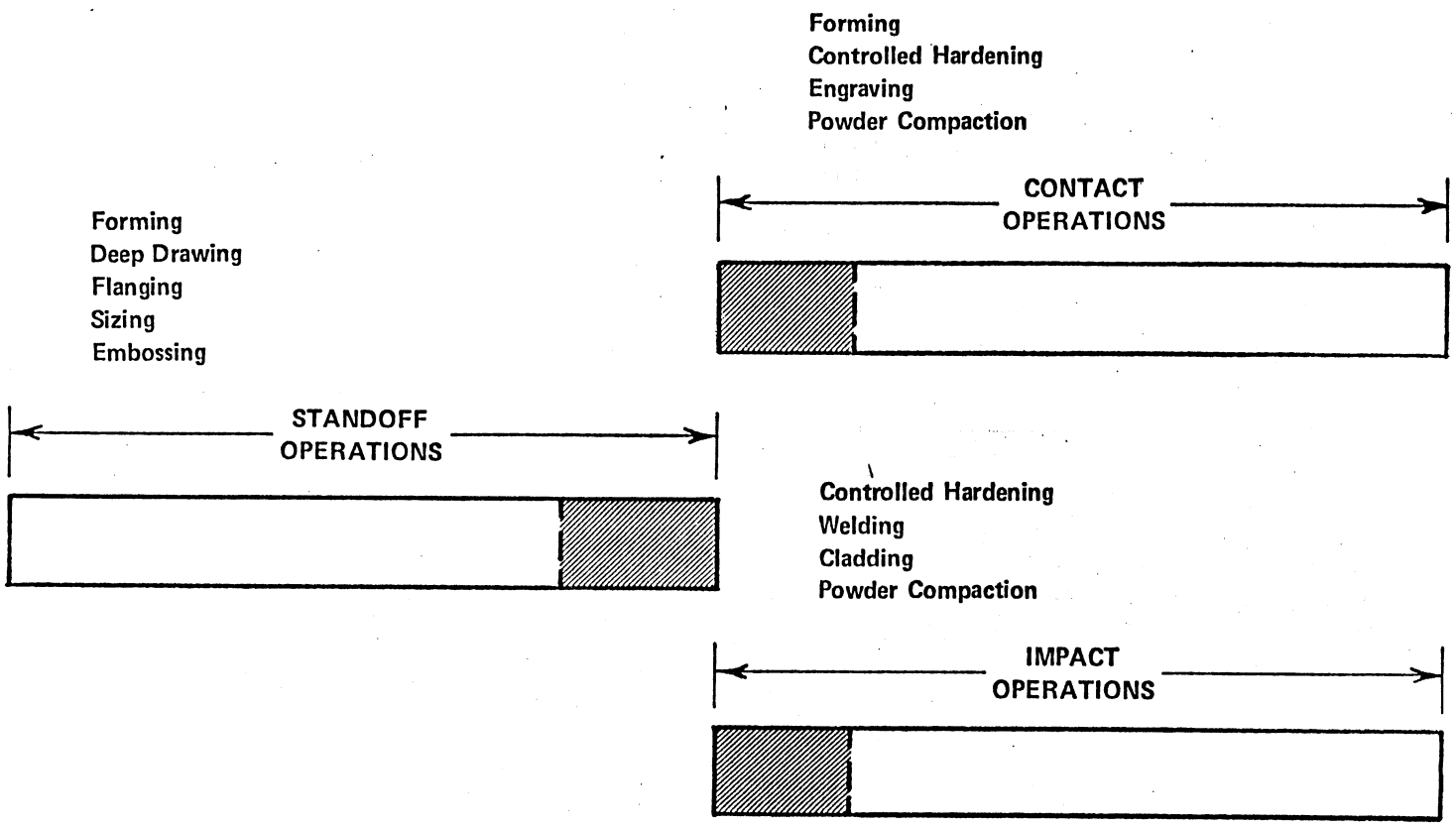

FIG. 3
MUNK & MORGAN/Chap. 3

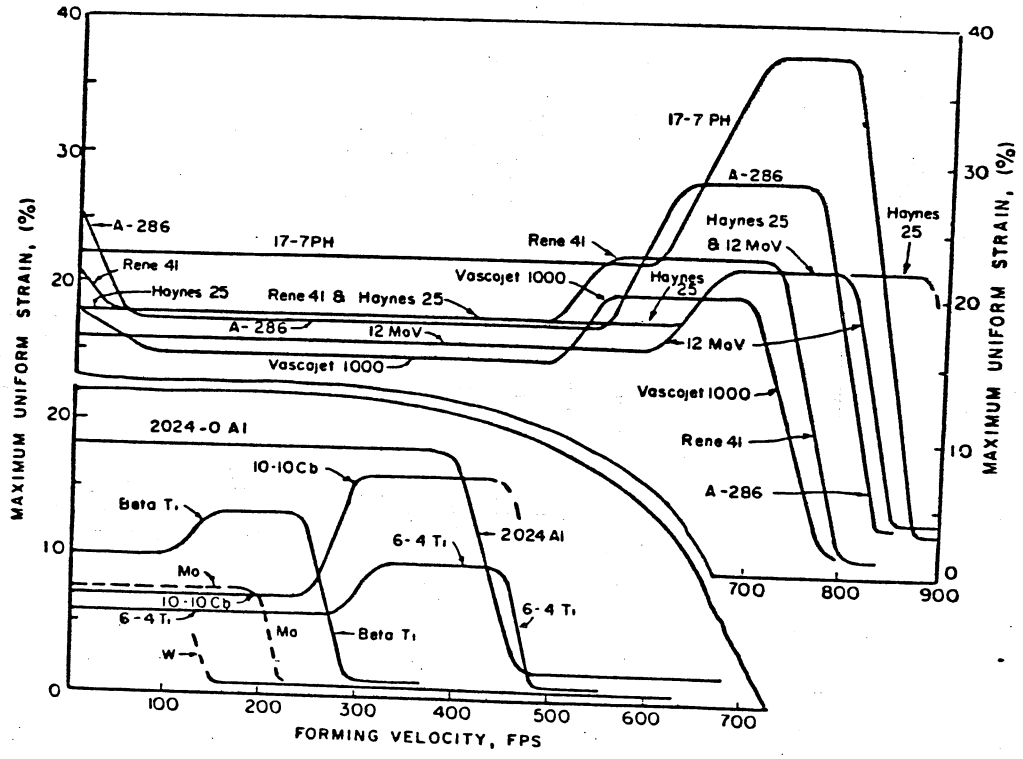

FIG. 4
MURR & MEYERS CHAP. 3

FIG. 5

MURR & MEYER
Chq. 3

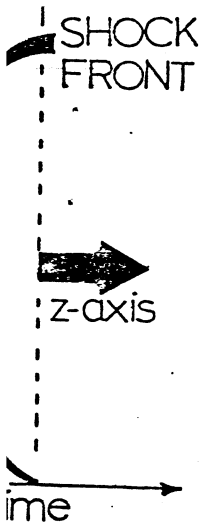

G (b)
& MEYERS/Chap 3

r

e
h
d
r plate

1.27 cm

2.54 cm

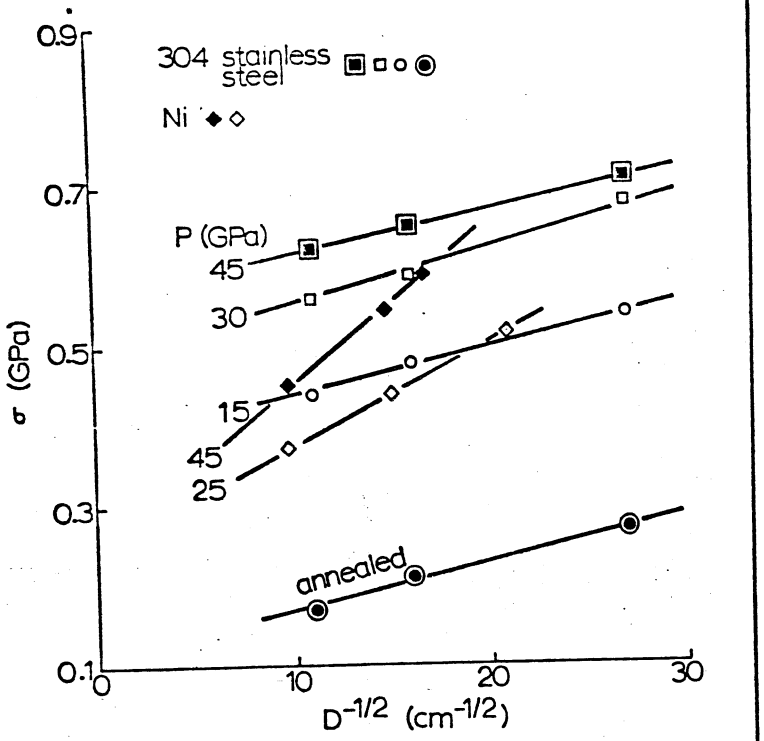

FIG. 7(a)
MURR & MEYERS

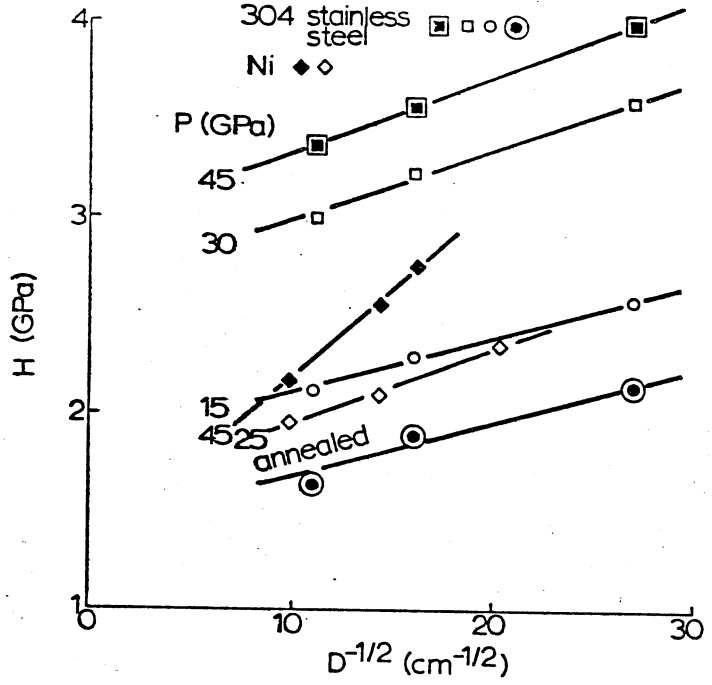

FIG. 7(b)
MURR & MEYERS

FIG. 8
MURR & MEYERS/Chp.3

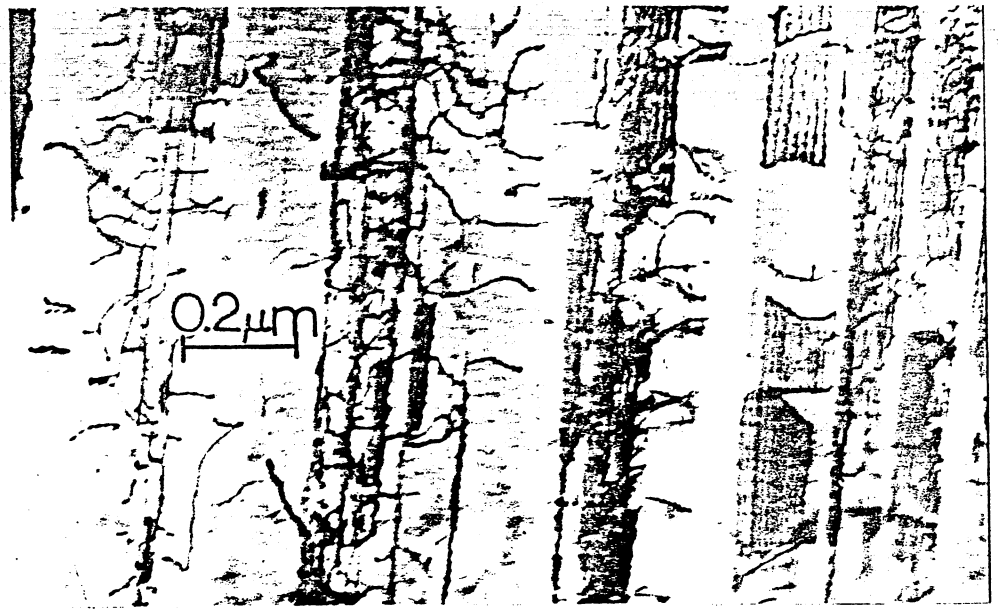

15 GPa

30 GPa

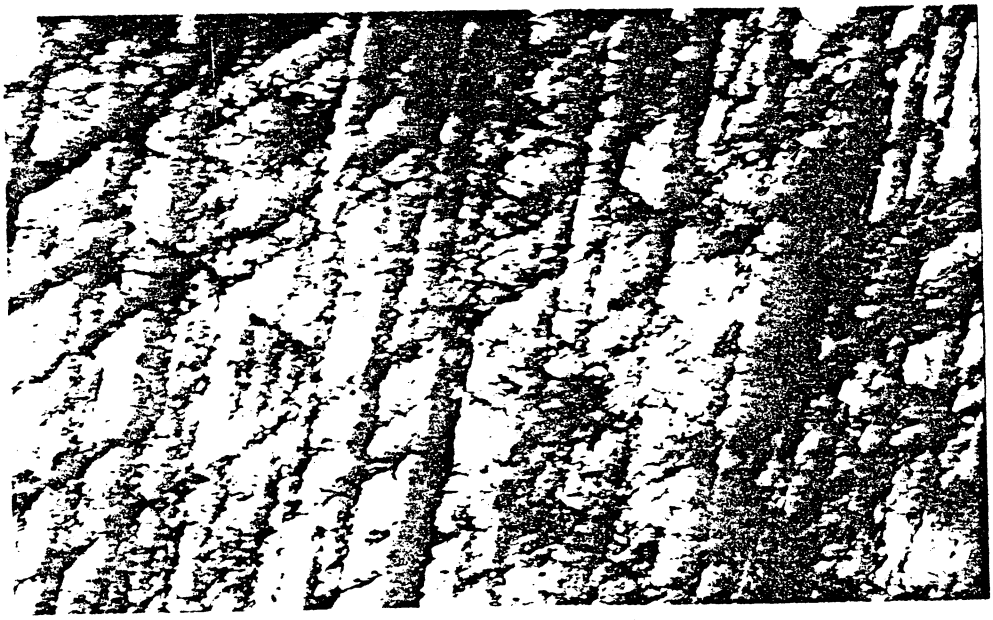

45 GPa

FIG. 9

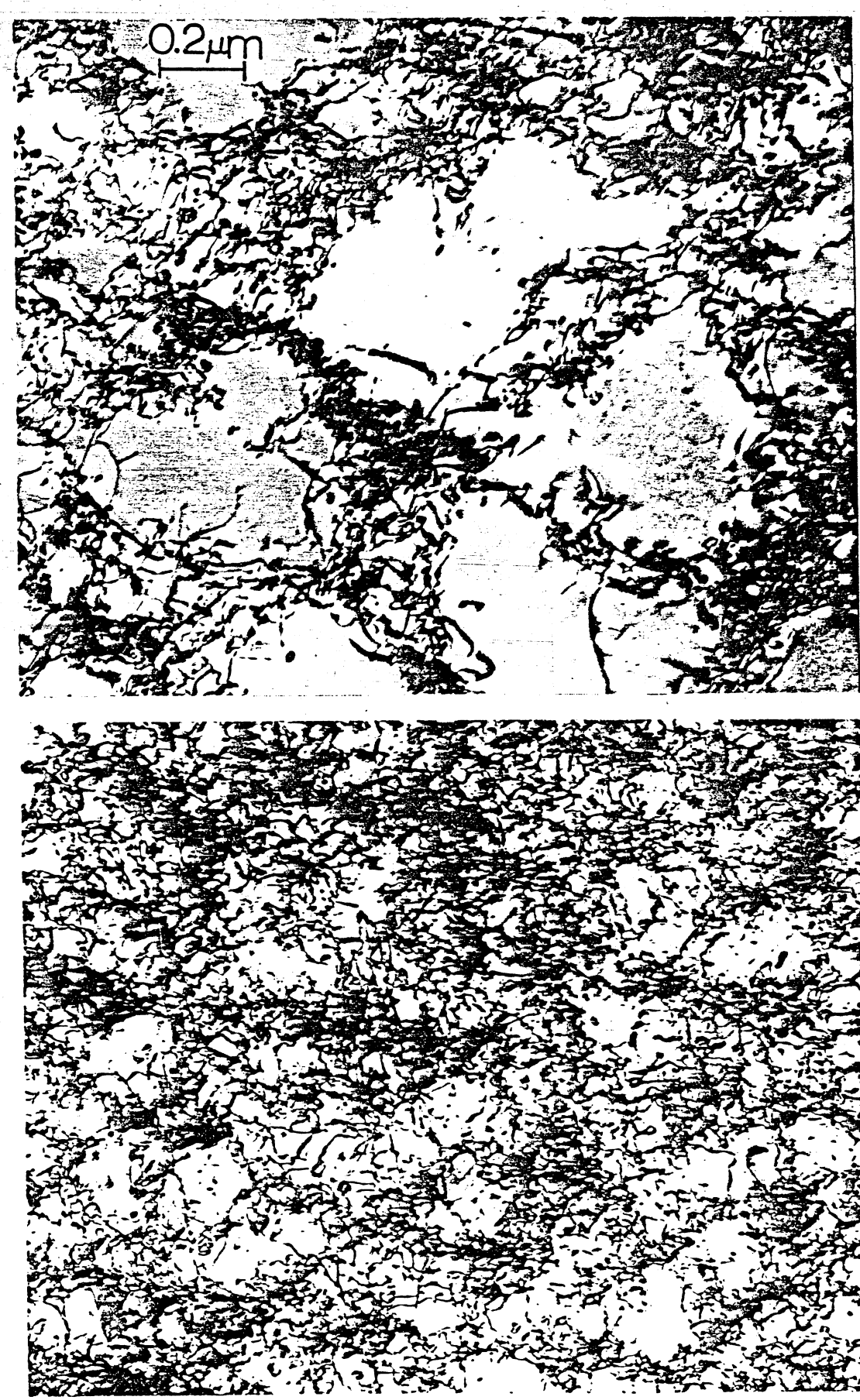

FIG. 10
MURR & MEYERS
Chap. 3

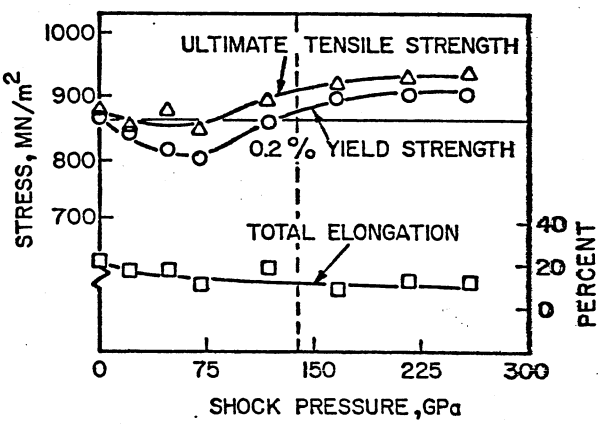

FIG. 11

MURR & MEYERS

Ch. 3

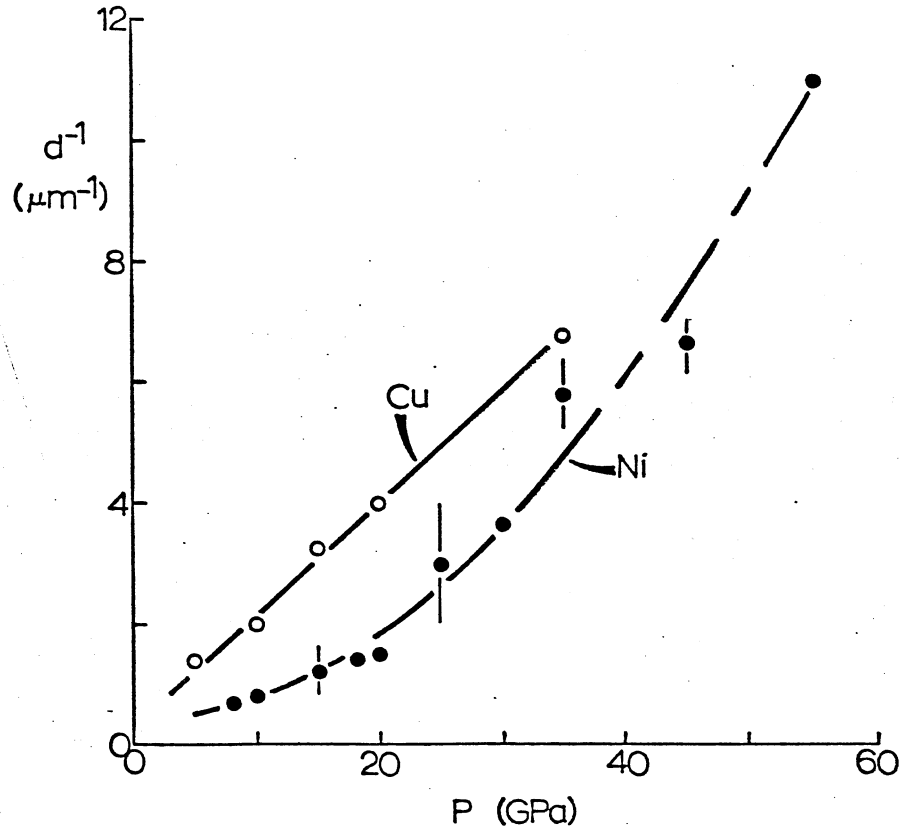

FIG. 12
URR & MEYERS
Chap. 3

FIG. 13
MURR & MEYERS
Ch. 3

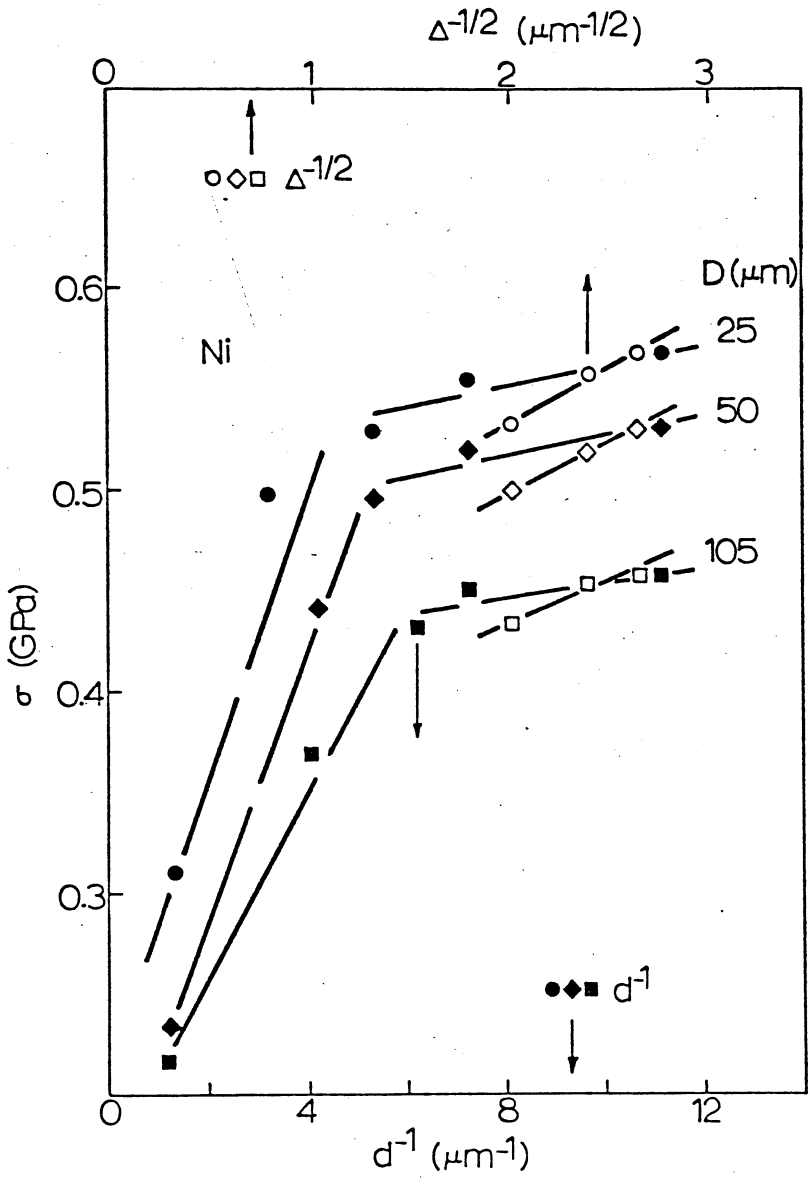

FIG. 14(a)
MURR & MEYERS

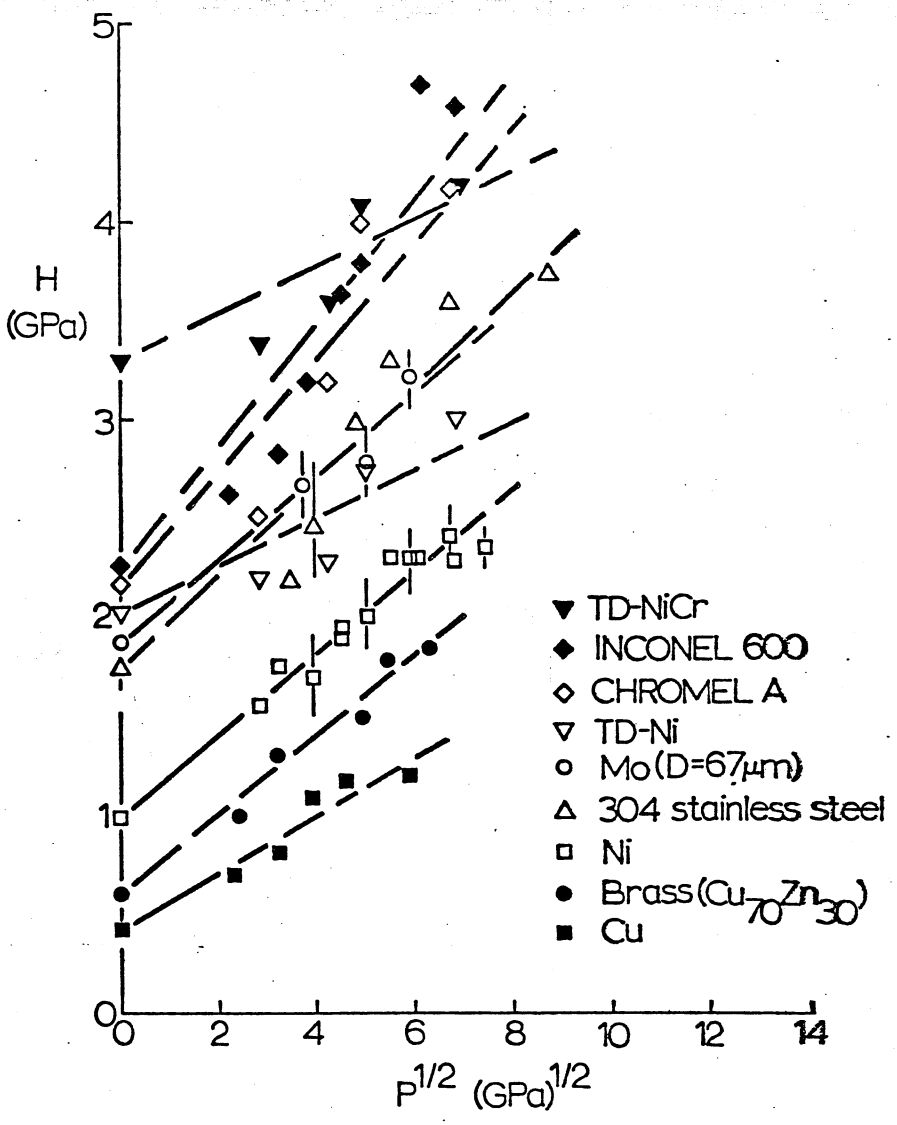

FIG. 14(b)
MURR & MEYERS

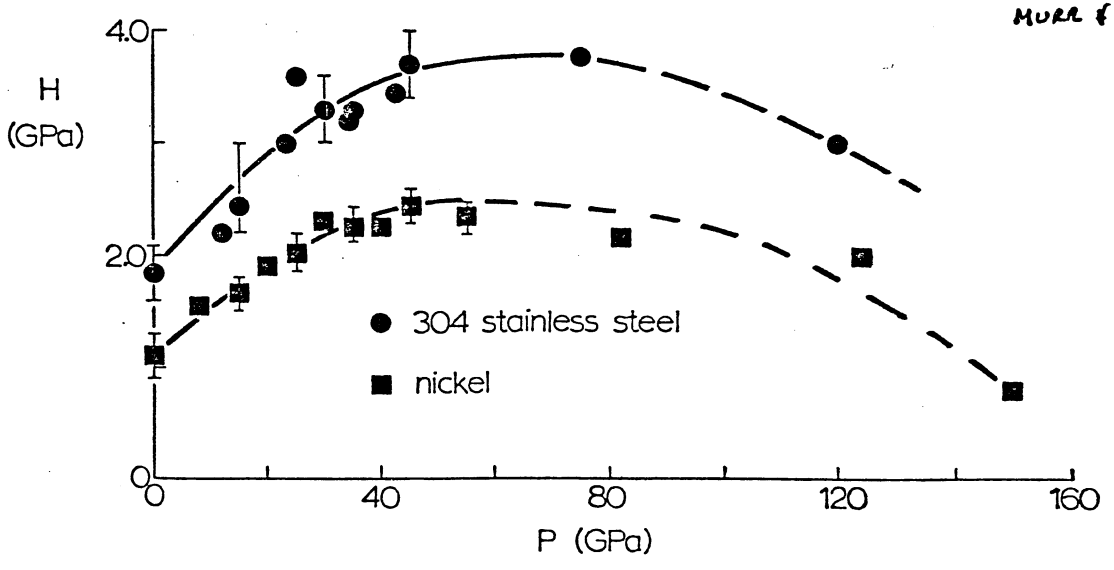

FIG. 15
MURR & MEYERS
Chap. 3

FIG. 16
MURR & MEYERS
Chap. 3

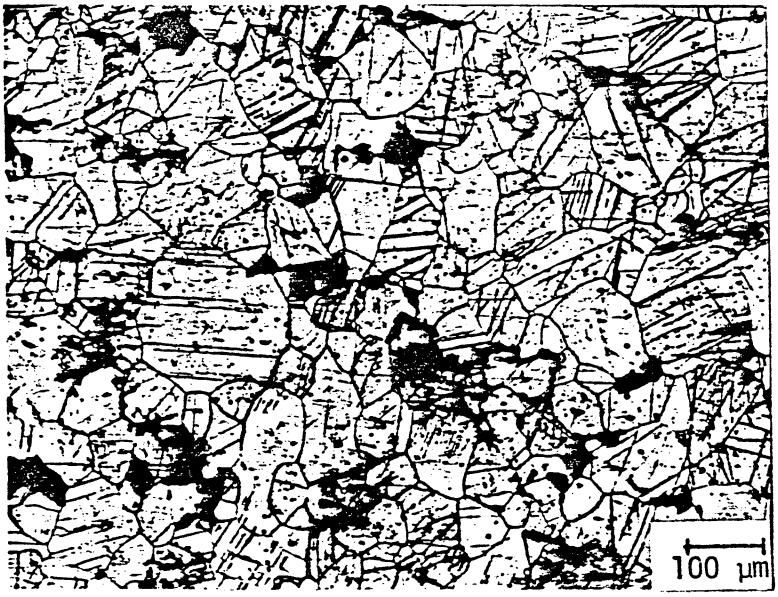

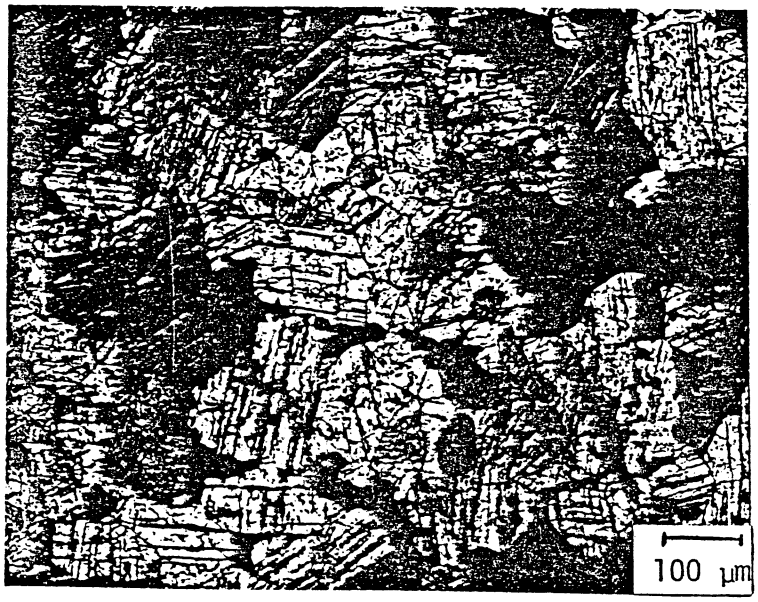

FIG. 17

MURR & MYERS

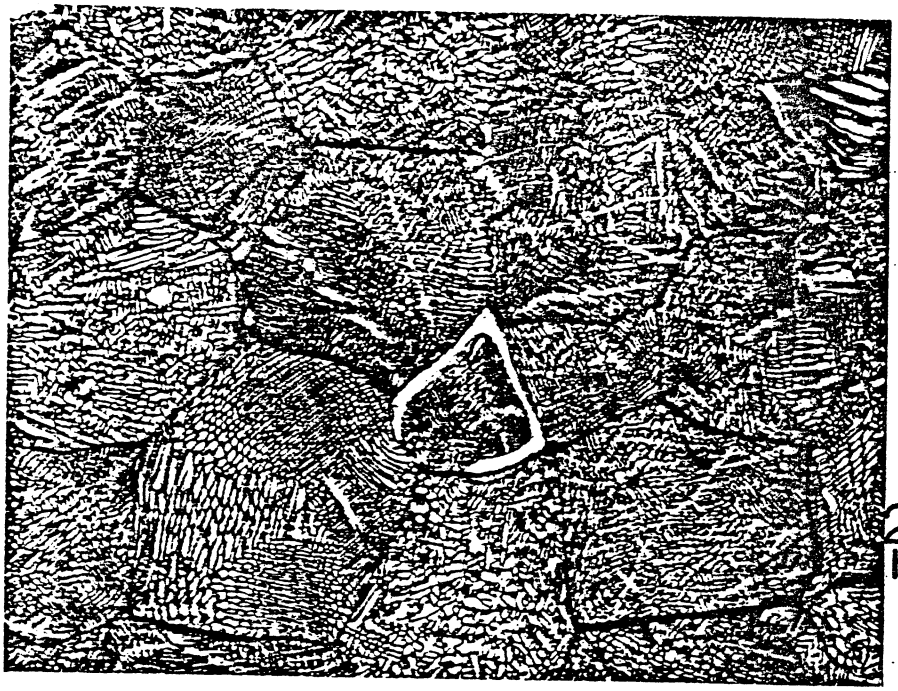

a

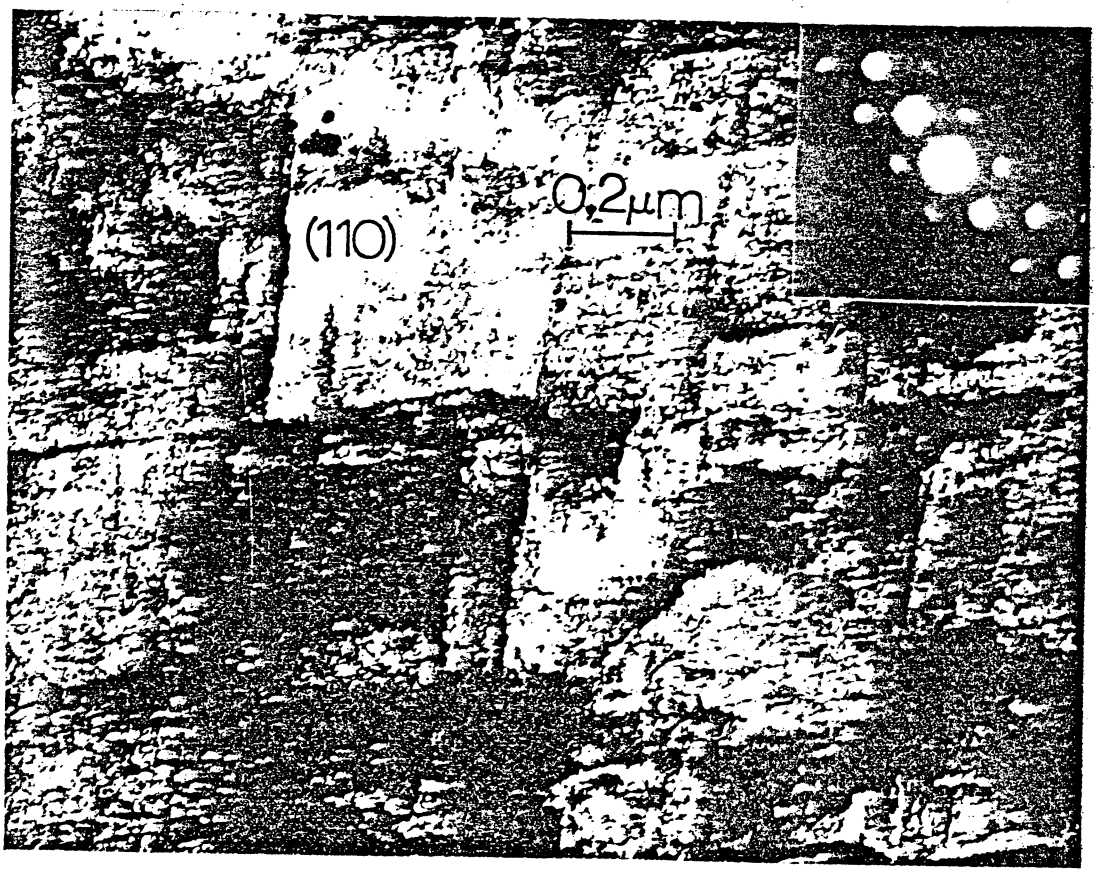

b

FIG. 18
MURR & McCOW / Chy:

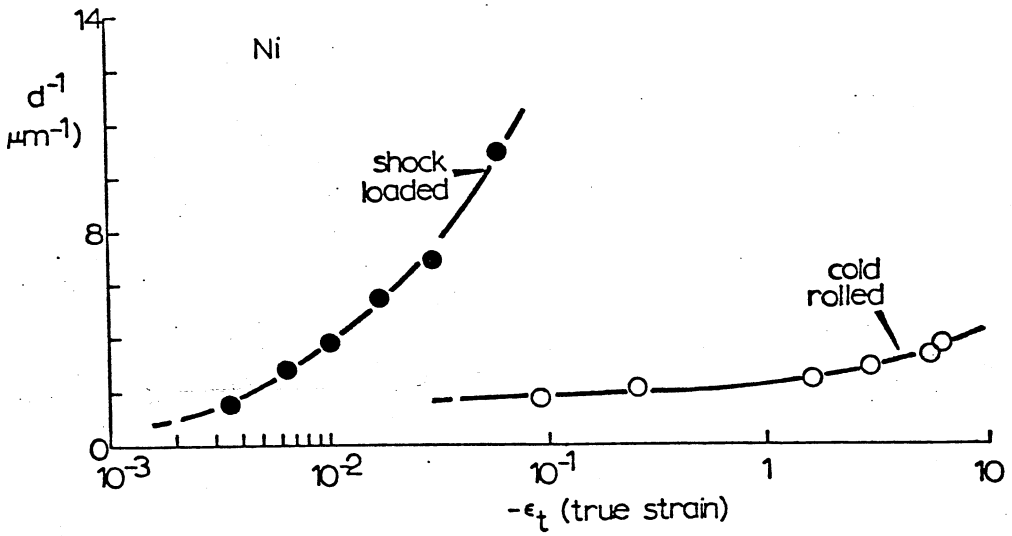

FIG. 19
MURR & MEYERS/Chp. 3

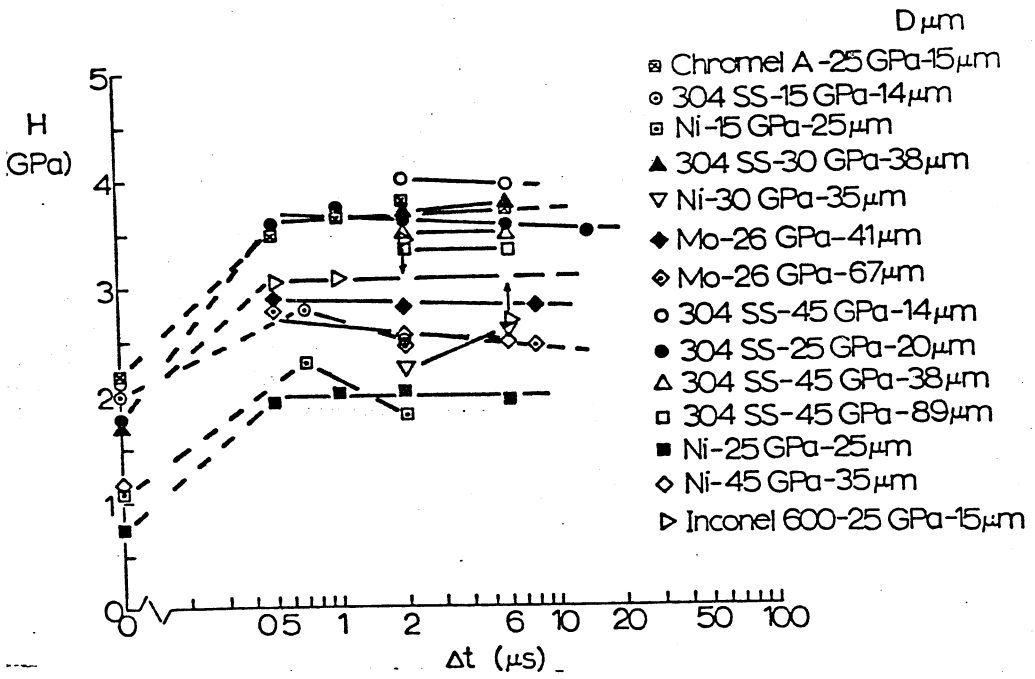

FIG. 20
MURR & MEYERS
Ch. 3

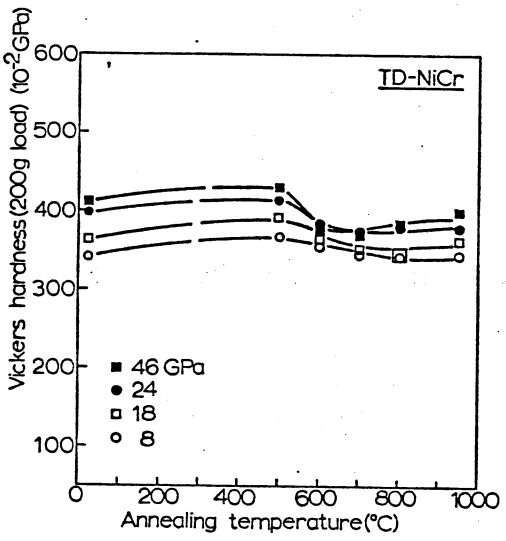

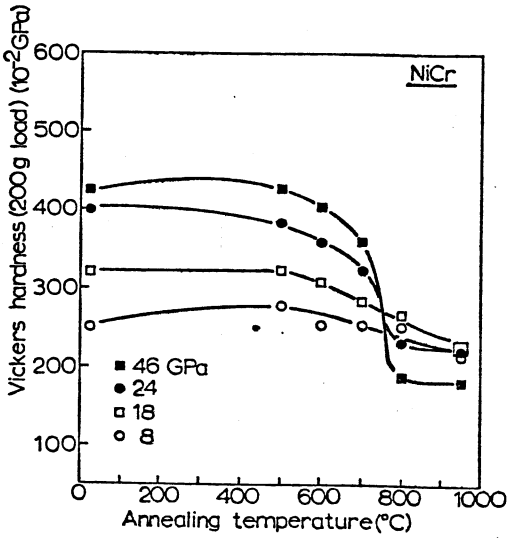

FIG. 21
MURR & MEYERS
Chap. 3

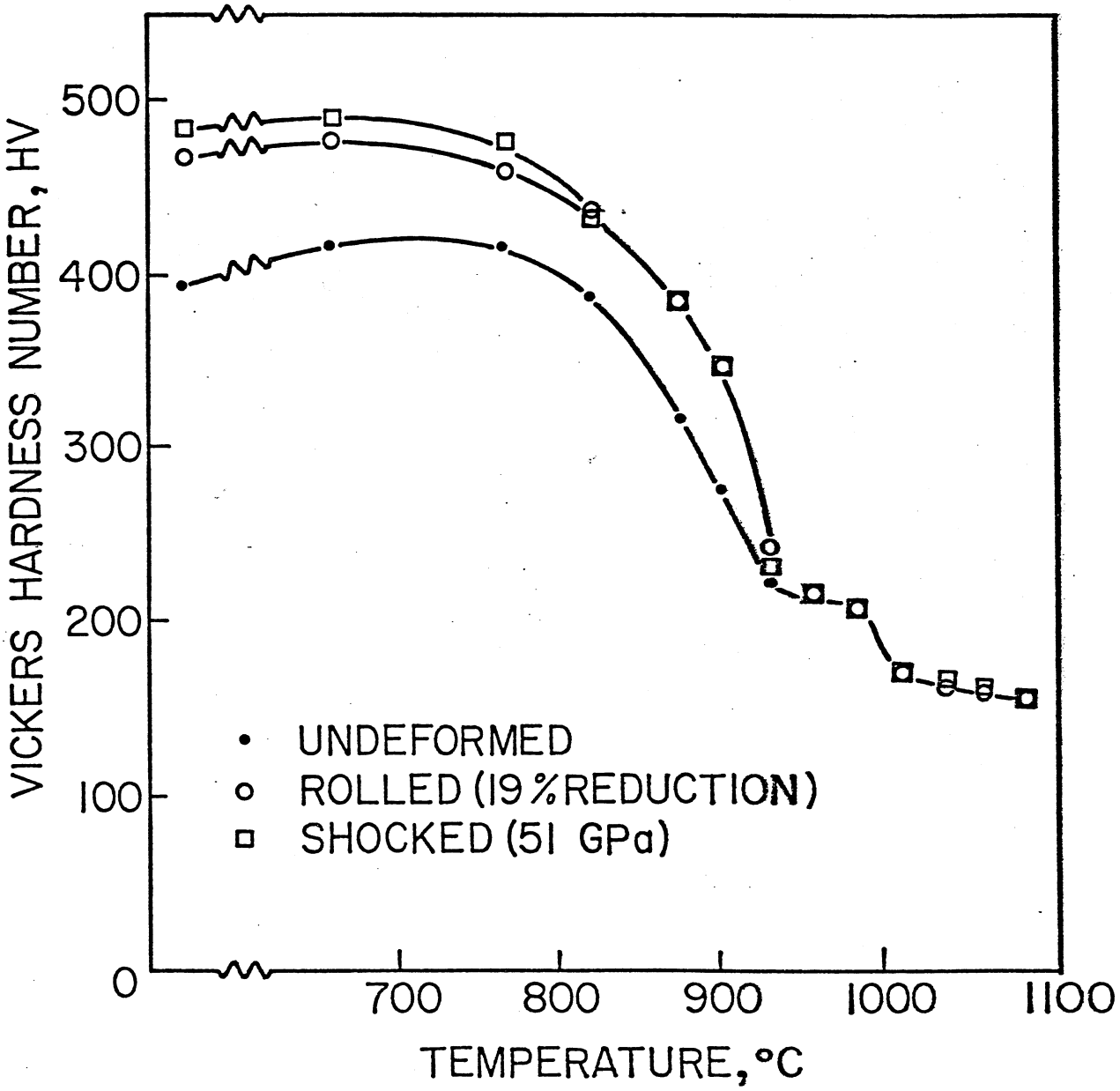

FIG. 22
MURR & MEYERS
Ch. 3

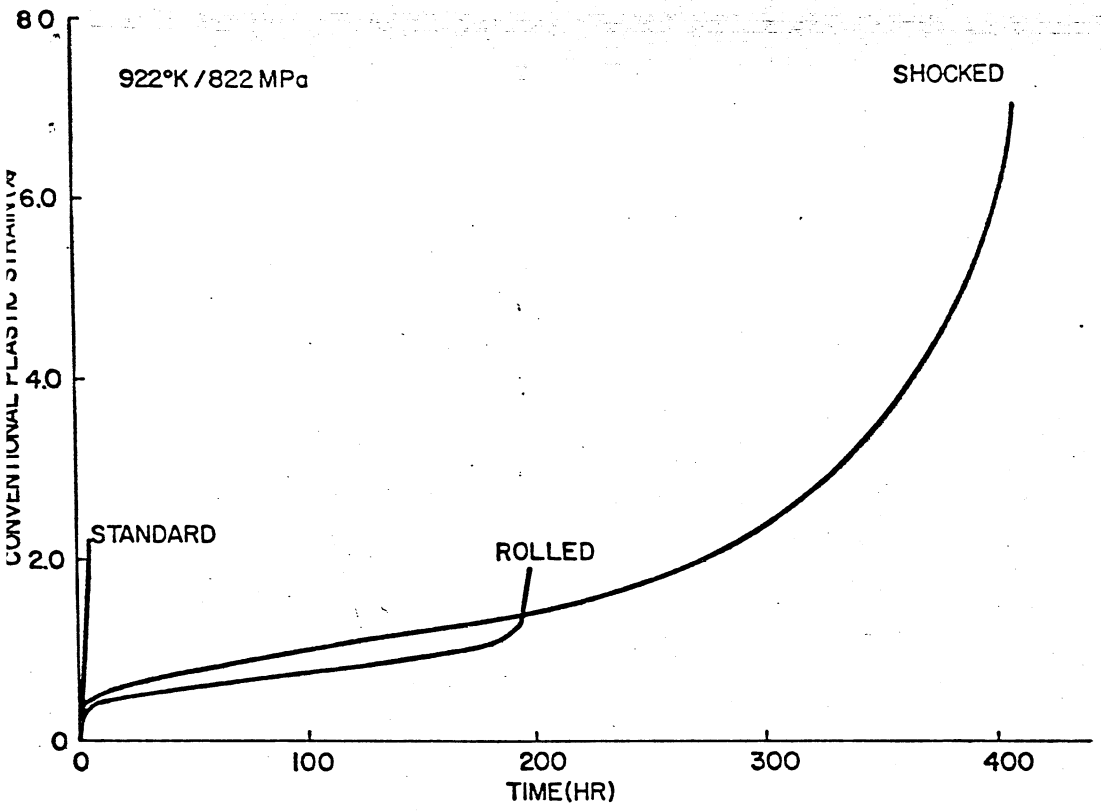

FIG. 23(a)
MURR & MEYERS
Chap. 3

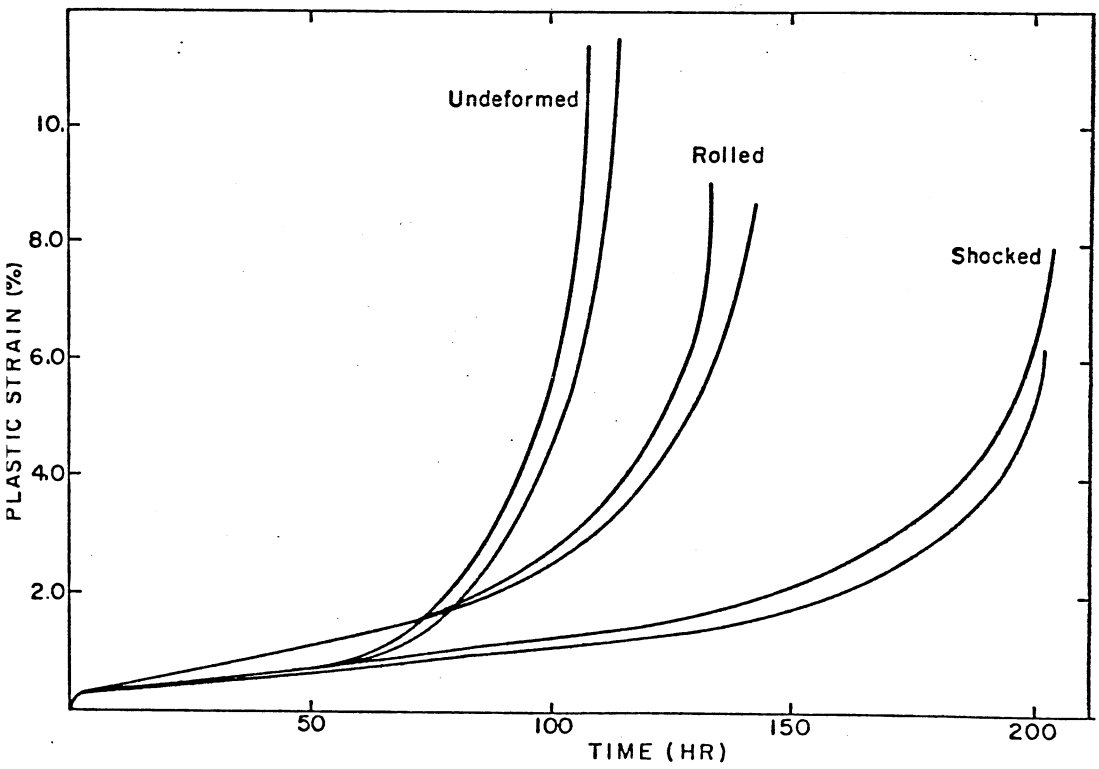

Chap. 23(b)
MURR & MEYERS
Chap. 3

FIG. 24
MURR & MEYERS

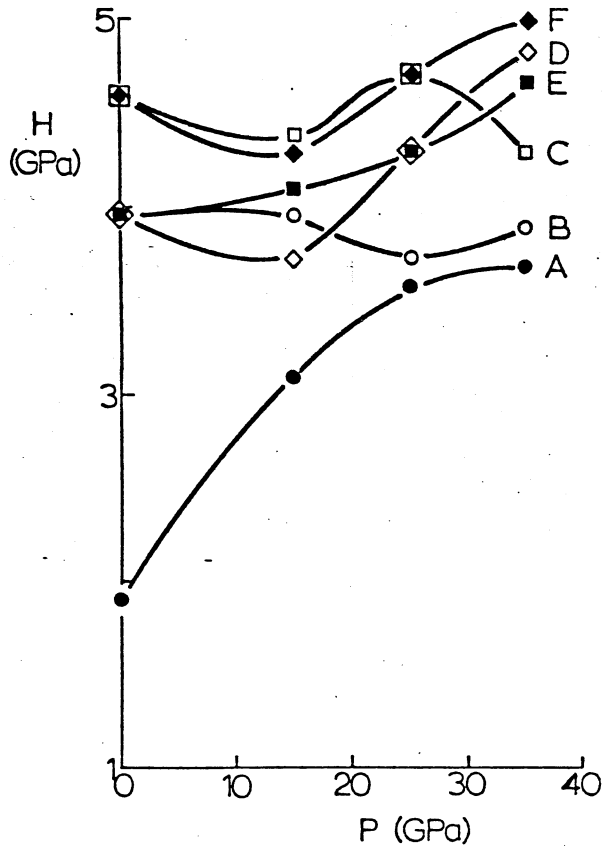

a

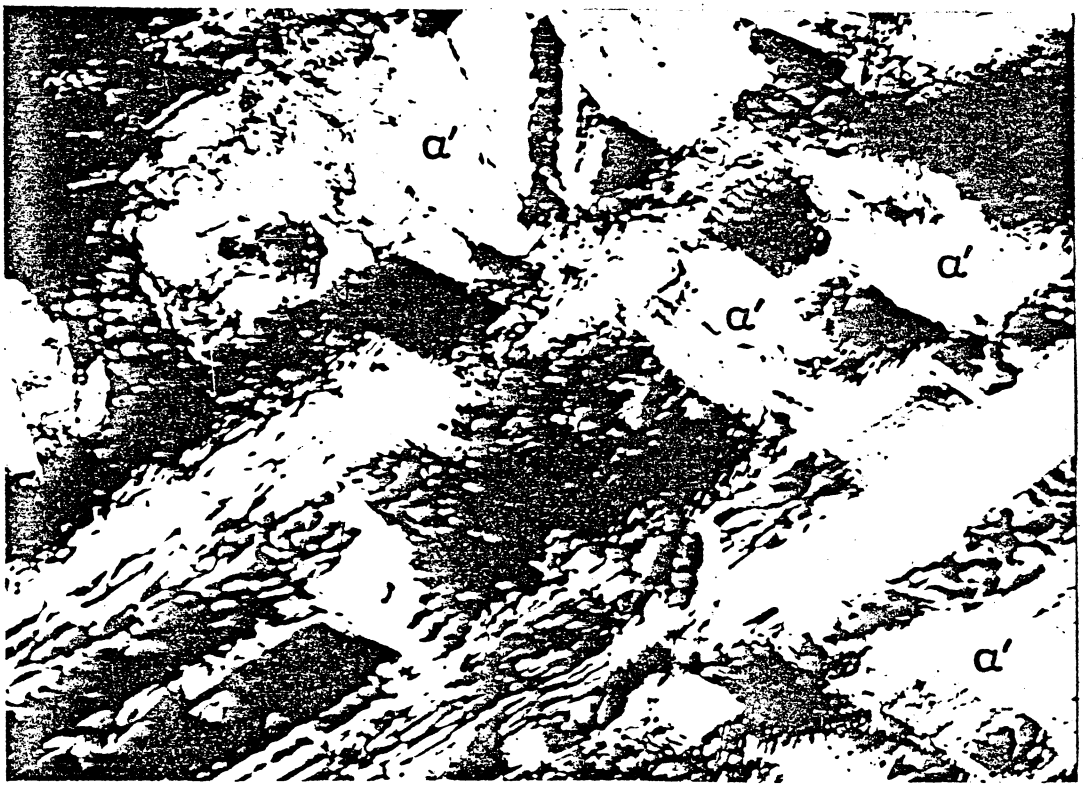

b

FIG. 25
MURR & MEYERS
Chp. 3

FIG. 26
MURR & MEYERS
Chp. 3

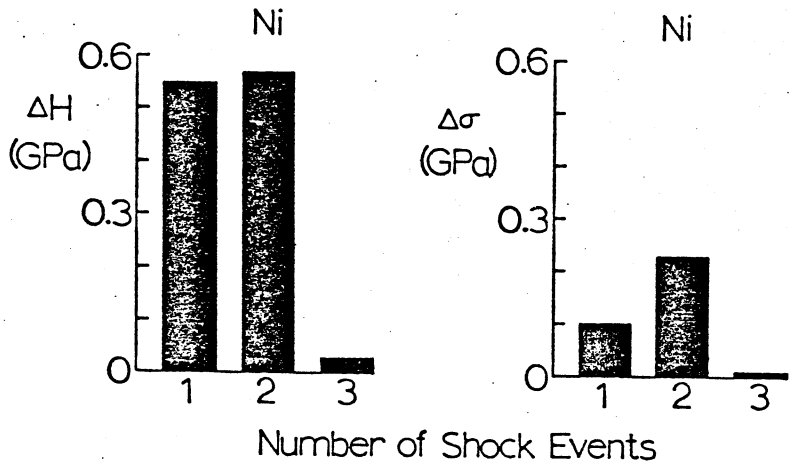

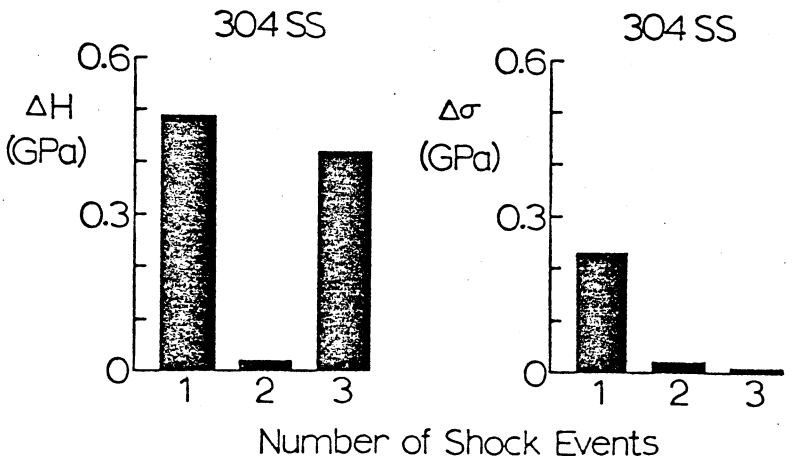

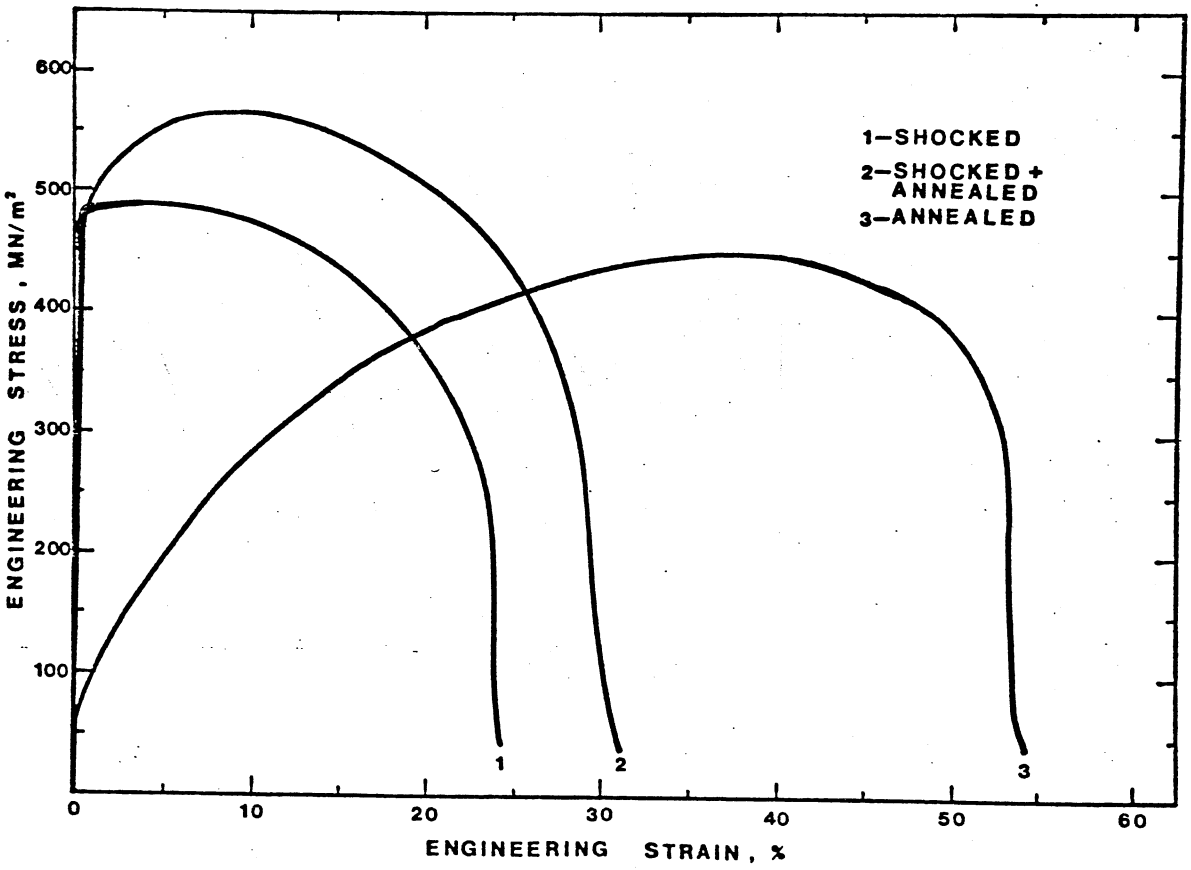

FIG. 27
MURR & MEYERS
Chap. 3

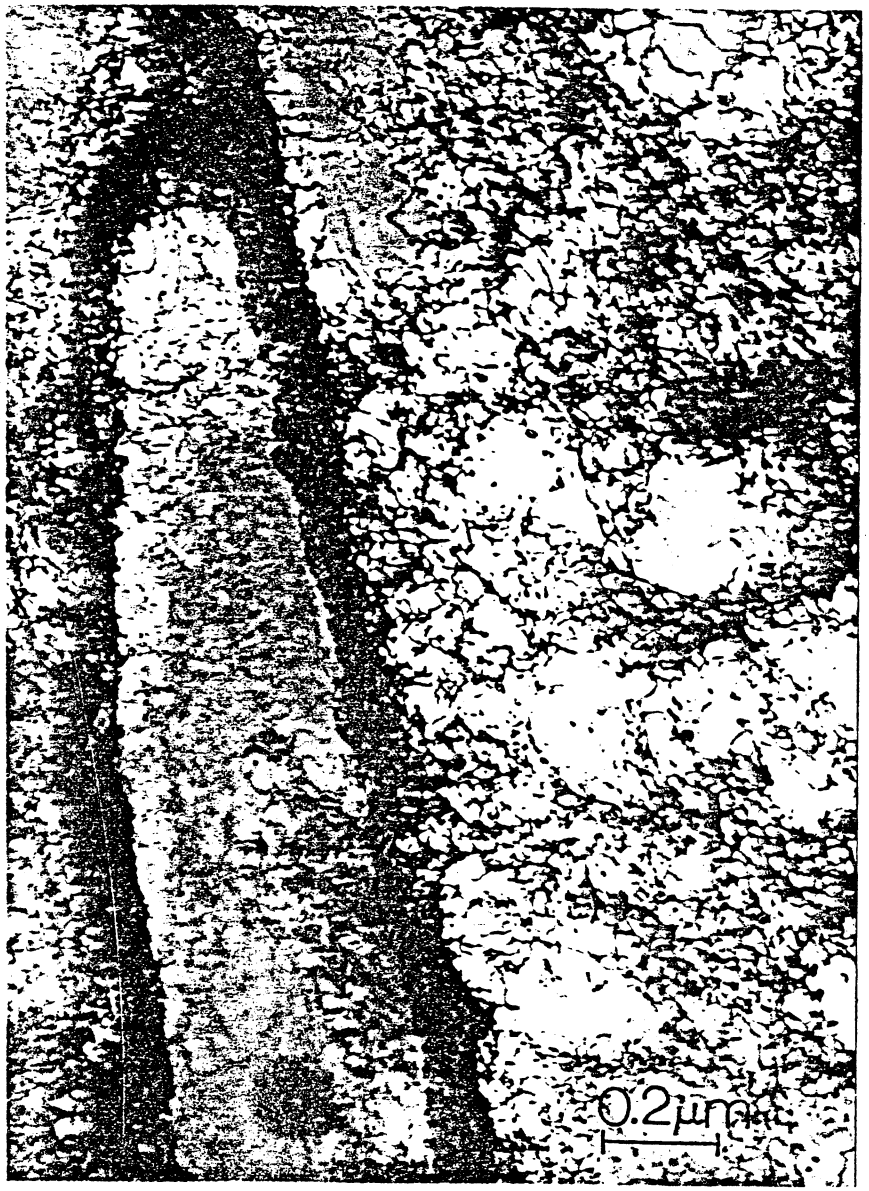

FIG. 28
MURR & MEYERS
Chp. 3